AD-A099 912 UNIVERSITY OF MANCHESTER INST OF SCIENCE AND TECHNOLO--ETC F/G 4/1
FIELD EXPERIMENTS ON THE OPTICAL, MICROPHYSICAL AND METEOROLOGI--ETC(U)
JAN 81 J LATHAM, M H SMITH DAJA37-79-C-0221

UNCLASSIFIED NL

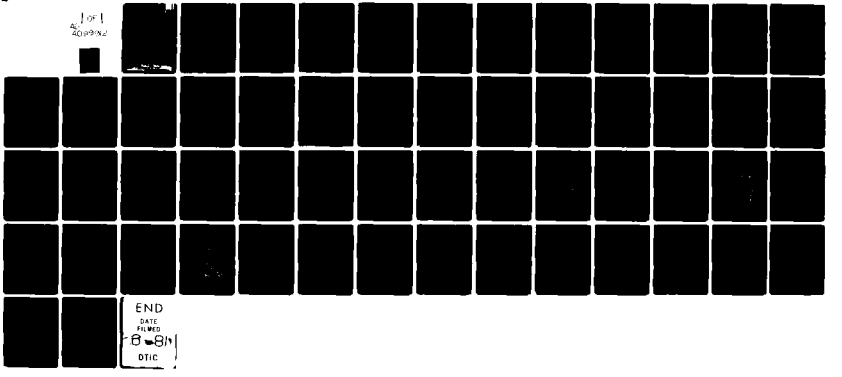

END
DATE FILMED
8-81
DTIC

The University of Manchester Institute of Science and Technology
PO BOX No 88 · SACKVILLE STREET · MANCHESTER M60 1QD
TELEPHONE 061-236 3311

(12)

LEVEL II

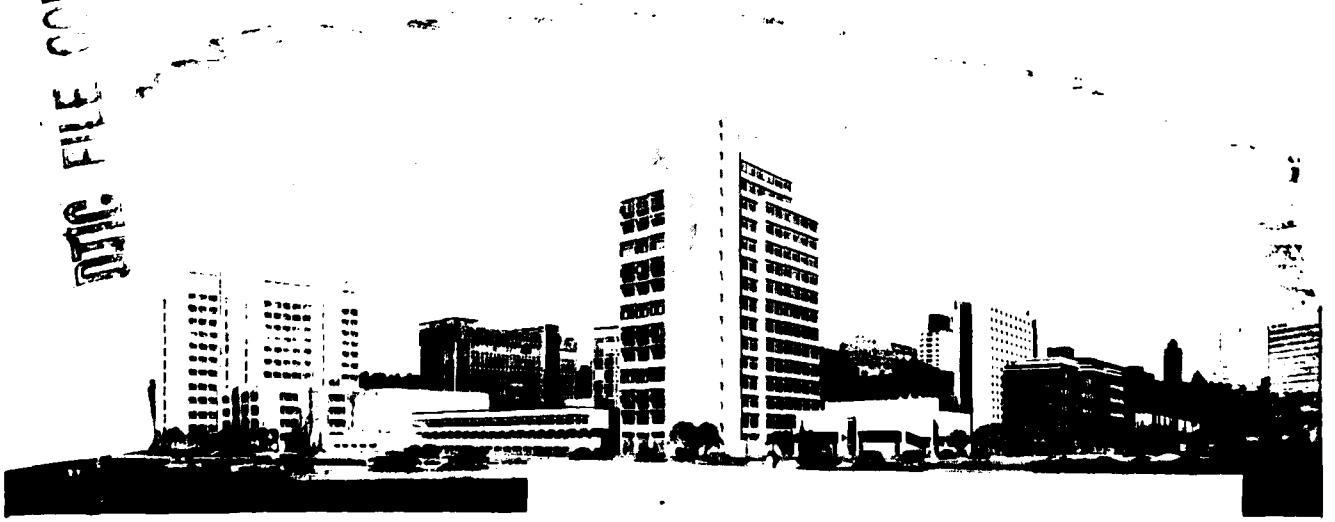

UNCLASSIFIED

SECURITY CLASSIFICATION OF THIS PAGE (When Data Entered)

R&D 2636-EN

REPORT DOCUMENTATION PAGE	READ INSTRUCTIONS BEFORE COMPLETING FORM
1. REPORT NUMBER	2. GOVT ACCESSION NO. AD-A099 912	3. RECIPIENT'S CATALOG NUMBER
4. TITLE (and Subtitle) Field Experiments on the Optical, Microphysical and Meteorological Characteristics of Natural Fogs and Clouds.	5. TYPE OF REPORT & PERIOD COVERED Final Technical Report Mar 79 - Jan 81
	6. PERFORMING ORG. REPORT NUMBER
7. AUTHOR(s) J. Latham and M. H. Smith	8. CONTRACT OR GRANT NUMBER(s) DAJA37-79-C-0221
9. PERFORMING ORGANIZATION NAME AND ADDRESS Department of Physics Univ. of Manchester Institute of Science and Technology, Manchester M60 1QD, U.K.	10. PROGRAM ELEMENT, PROJECT, TASK AREA & WORK UNIT NUMBERS IT161102BH57-01
11. CONTROLLING OFFICE NAME AND ADDRESS USARDSG-UK Box 65 FPO New York, NY 09510	12. REPORT DATE January 1981
	13. NUMBER OF PAGES 52
14. MONITORING AGENCY NAME & ADDRESS (if different from Controlling Office) US Army Atmospheric Sciences Laboratory White Sands Missile Range, NM 88002	15. SECURITY CLASS. (of this report) Unclassified
	15a. DECLASSIFICATION/DOWNGRADING SCHEDULE

16. DISTRIBUTION STATEMENT (of this Report)

Approved for public release; distribution unlimited

17. DISTRIBUTION STATEMENT (of the abstract entered in Block 20, if different from Report)

18. SUPPLEMENTARY NOTES

19. KEY WORDS (Continue on reverse side if necessary and identify by block number)

Fog, Clouds, Aerosols, Liquid aerosols, microphysics, cloud physics, condensation, droplet spectra, droplet growth, meteorology, cloud meteorology, fog meteorology

20. ABSTRACT (Continue on reverse side if necessary and identify by block number)

The experimental program incorporates measurements of condensation nuclei concentrations and associated meteorological parameters made within the air feeding into clouds, as well as within such clouds. Instruments include modifications of Keily probe electrostatic disdrometers, PMS spectrometer probes, a Mee CCN counter and a PMS ASASP probe. A passive optical scattering instrument has also been used, in conjunction with a Barnes transmissometer operating at about 11.0 μm. Data for a variety

DD FORM 1 JAN 73 1473 EDITION OF 1 NOV 65 IS OBSOLETE S/N 0102-LF-014-6601

UNCLASSIFIED

SECURITY CLASSIFICATION OF THIS PAGE (When Data Entered)

20. Cont.

of conditions and meteorological situations are presented. Theoretical work has included the development of an airflow model capable of predicting the microphysical properties of clouds over the summit of Great Dun Fell from a knowledge of the relevant parameters concerning the air parcels from which the clouds are formed. Computational studies have been made of the role of undersaturated air upon droplet size distributions.

FIELD EXPERIMENTS ON THE OPTICAL, MICROPHYSICAL AND METEOROLOGICAL CHARACTERISTICS OF NATURAL FOGS AND CLOUDS.

(9) FINAL TECHNICAL REPORT, Mar 79 - Jan 81

(11) Jan 81 (12) 56

Contract No (15) DAJA37-79-C-0221

(10) (16) 1T161102 [illegible] (17) 01

Professor J. Latham & M. H. Smith
Physics Department
UMIST
Manchester M60 1QD

J Latham
Principal Investigator

M H Smith
Project Co-ordinator

AD A100 330

INTRODUCTION

Considerable progress has been made toward a comprehensive understanding of the formation, development and microphysical structure of clouds and fogs formed over the summit of Great Dun Fell together with their related absorption of radiation at optical and infra-red wavelengths.

The experimental program incorporates measurements of condensation nuclei concentrations and associated meteorological parameters made within the air feeding into these clouds, utilizing a mobile laboratory, in addition to microphysical and transmission measurements made within such clouds at the summit of Great Dun Fell. Equipment available for these studies which has been developed or modified for ground-based usage includes Keily probe electrostatic disdrometers and two PMS spectrometer probes (FSSP) for the measurement of cloud droplet distributions together with a modified Mee CCN counter and a PMS ASASP probe for measuring the smaller aerosol particles. A passive optical scattering instrument of novel design for the simultaneous measurement of visibility and cloud liquid water content has been developed and utilized in field studies at Great Dun Fell. Asscciated measurements of the transmission of infra-red radiation at about 11μm have been made with a Barnes transmissometer.

A comparison of measured extinction coefficient values for radiation of this wavelength with values calculated from microphysical measurements is provided in Section III.

Theoretical work has included the development of an airflow model capable of predicting the microphysical properties of clouds over the summit of Great Dun Fell from a knowledge of the relevant parameters concerning the air parcels from which the clouds are formed. In addition, computational studies have been made of the role of entrainment of undersaturated air upon the droplet size distribution for situations relevant to the field

investigations. This investigation of turbulent mixing is described in Section I of this report. Section II provides a detailed comparison of the theoretical cloud model with field observations made in differing atmospheric situations.

The work presented in this report, whilst still in its preliminary stages and capable of much further refinement, has nevertheless shown that the microphysical properties of clouds formed over Great Dun Fell may be predicted from a knowledge of the parameters of the air below cloud base with a notable degree of accuracy. Furthermore, the initial investigations of the transmission of infra-red radiation through these clouds suggest that this parameter may be directly related to their microphysical properties. Thus the prospect of being able to estimate the attenuation characteristics likely to arise during the formation and development of clouds and fogs from the preceding meteorological conditions appears increasingly realistic.

I. TURBULENT MIXING MODEL

We have made some calculations to investigate the influence of turbulent entrainment of environmental air upon the adiabatic cloud droplet spectrum. We assume the turbulent mixing to be roughly represented by diffusion, with a constant coefficient K ($m^2 s^{-1}$) determined on dimensional grounds from the original spectral scale λ (m) of the entrained parcel, and ϵ ($m^2 s^{-3}$), the rate of dissipation of turbulent energy within the cloud. It should be noted that this approximation is best suited to the case where λ is much greater than the characteristic eddy size within the clouds: $K = (\lambda^4 \epsilon)^{\frac{1}{3}}$. Neglecting buoyancy effects and assuming the turbulent motions transport sensible heat, liquid water and water vapour simultaneously, we have

$$\frac{\delta T}{\delta t}(\underline{R},t) - K\nabla^2 T(\underline{R},t) = \dot{T}_{evap}(\underline{R},t) \qquad (1)$$

$$\frac{\delta L}{\delta t}(\underline{R},t) - K\nabla^2 L(\underline{R},t) = \dot{L}_{evap}(\underline{R},t) \qquad (2)$$

$$\frac{\delta \rho}{\delta t}(\underline{R},t) - K\nabla^2 \rho_v(\underline{R},t) = \dot{\rho}_{evap}(\underline{R},t) \qquad (3)$$

and

$$\dot{L}_{evap}(\underline{R},t) = -4\pi \int_0^\infty n(r,\underline{R},t) \frac{r^2}{r+a} \left[S(\underline{R},t) - \frac{A}{r} + \frac{B}{r^3}\right] dr \qquad (4)$$

$$\dot{T}_{evap}(\underline{R},t) = -\frac{\mathscr{L}}{\rho c_p} \dot{L}_{evap}(\underline{R},t) \qquad (5)$$

$$\dot{\rho}_{evap}(\underline{R},t) = -\dot{L}_{evap}(\underline{R},t) \qquad (6)$$

$$S(\underline{R},t) = \left(\frac{\rho_v(\underline{R},t)}{\rho_s(\underline{R},t)} - 1\right).100 \qquad (7)$$

$$\rho_s(\underline{R},t) = 1.8.10^{-9} \exp\left(\frac{-5400}{T(\underline{R},t)}\right) \quad (g\ m^{-3}) \qquad (8)$$

$n(r,\underline{R},t)dr$ is the number (m^{-3}) of drops at $(\underline{R},t)$ with radii in the interval $r, r+dr$, and a is a diffusion length we have put equal to 5μm. $A = 2M_w\sigma/RT\rho_w$, $B = 3\nu M_w m_s/4\pi\rho_w M_s$, r is the droplet radius, M_w and M_s the molecular weights of water and the aerosol,

ν the number of ions per aerosol molecule, σ the surface tension of the aqueous solution drop against air, ρ_w the density of water, L the latent heat of evaporation and R the universal gas constant. We assume that all droplets have identical nuclear mass m_s. While these equations could be made more precise by improving the expressions for ρ, ρ_s and the droplet growth equations, such changes were deemed unnecessary at this stage in view of the very approximate relationship between the diffusion problem and the mixing process we are studying.

The numerical computations assume that a spherical blob of radius λ is placed at t=0 at the centre of a spherical cloud shell of outer radius R_{MAX}. Because buoyancy can be neglected spherical symmetry is preserved throughout the diffusion phase change process. We assume the boundary conditions

$$\frac{\delta T}{\delta t}(l,t) = \frac{\delta L}{\delta l}(l,t) = \frac{\delta \rho_v}{\delta l}(l,t) = \frac{\delta n}{\delta l}(l,r_j,t) = 0$$

at $l = R_{MAX}$ for all t.

$T(0,t)$, $L(0,t)$, $\rho_v(0,t)$ and $n(0,r_j,t)$ are finite, for all r_j and t.

In the calculation, diffusion and phase change proceed sequentially. That is, at the beginning of each time step all parameters are known at each spatial grid point l_i. The grid spacing chosen was $\Delta l = l_{i+1} - l_i = \lambda/10$, where $l_i = (i=1)\Delta l$. Diffusion proceeds via a forward differencing algorithm with the right-hand-sides of the first three equations equal to zero for a time $\Delta t = (\Delta l)^2/6K$ set for numerical stability. Then all motion stops and phase change (evaporation or condensation) takes place at each grid point according to equations (4) to (8). This continues for a time Δt after which the time variable is advanced by Δt and the diffusion step repeated. The time step for the phase change equations was set equal to $0.1\Delta t$ and was always less than 0.1s.

The stability of the diffusion algorithm was checked for each run by comparing the results of the diffusion calculation in the absence of phase change with the analytical solution for the spherically symmetric problem with the zero flux boundary condition. For all runs considered the numerical and analytical solution agreed to within 0.1%

II. FIELD STUDIES OF THE EFFECT OF ENTRAINMENT UPON THE STRUCTURE OF CLOUDS AT GREAT DUN FELL

ABSTRACT

A description is given of experiments performed to investigate the effect of the entrainment of undersaturated air upon the microphysical structure of cap clouds at Great Dun Fell, Cumbria. The results obtained are compared with the predictions of simple theoretical models. Three case studies are presented: in case I the properties of the cloud were essentially adiabatic; II provided evidence for mixing intermediate between the homogeneous and extreme inhomogeneous types; in III the mixing was extremely inhomogeneous. Consistent with this picture, the time constant for turbulent erosion of the entrained parcels of air is significantly greater in case III than in case II. Spectral changes predicted by a model of turbulent entrainment (Baker and Latham, 1981) agree well with observation.

I. INTRODUCTION

Baker and Latham (1979) and Baker, Corbin and Latham (1980) have presented calculations which suggest that the influence of dry air entrainment on the microphysical structure of a cloud is strongly dependent on the ratio of the time constants for turbulent diffusion of entrained air, τ_T, and for the evaporation of drops in response to the undersaturation τ_E. Measurements of microphysical properties of clouds enveloping Great Dun Fell (GDF) in Cumbria described by Blyth et al (1980) suggested that entrainment has an appreciable effect on these clouds. In addition, the indications were that for the clouds sampled the effect of the mixing is closer to that of the extreme inhomogeneous description of Baker and Latham, ($\tau_T/\tau_E >> 1$), than the classical description, which implies that $\tau_T/\tau_E << 1$.

In this paper three detailed case studies are discussed which throw additional light on the effect of entrainment upon the properties of clouds over Great Dun Fell.

In case I entrainment effects appeared to be negligible and the cloud was thus essentially adiabatic. In cases II and III the liquid water contents were substantially sub-adiabatic, indicating that significant entrainment of undersaturated environmental air occurred. In each case a simple dynamical and microphysical model of the cloud is used to relate the microphysical measurements to the meteorological conditions. An attempt is made to assess the influence of entrainment upon the cloud properties in terms of a simple diffusive model of the mixing process developed by Baker and Latham (1951).

2. INSTRUMENTATION AND EXPERIMENTAL PROCEDURES

The basic arrangements and procedures were similar to those employed by Blyth et al (1980) so will not be reproduced here. We merely outline the instrumentation and draw attention to additional devices employed.

At the summit of the hill drop spectral data were obtained using the Keily Probe (KP) (Corbin et al 1978), cases I and III, and a PMS Axially Scattering Spectrometer Probe (ASSP) (Ryder 1976), case II, and for a small period of case III. Occasional measurements of drop concentration and size distribution were made using a pulsed Laser Holography System (Conway et al 1980, 1981). A high frequency acoustic sounder (Moulsley and Cole 1979) was employed to monitor the height of the lowest inversion base, taken as cloud top height (see e.g. Caughey et al 1978, 1981).

The ASSP-100 is regarded as primarily a droplet sizing instrument. A comparison was carried out between droplet spectra from the holographic laser system and the ASSP-100 (see Conway et al 1981). Good agreement was obtained for both mean radius and spectral shape. Droplet concentrations (and hence liquid water content) are, however, known to be over-estimated by our ASSP. Comparison with droplet concentrations deduced from the holographic technique during the present studies resulted in a correction factor of 0.5 for the ASSP droplet counts and this has been applied to the whole data set. This figure is in good agreement with that deduced from other studies of ASSP measured liquid water contents and those from other instruments (Kitchen, 1979, Slingo et al 1981).

The results obtained with the Keily probe and the corrected PMS ASSP data were compared in detail during the period 1635-1650 on 15 May (Case III). The cloud properties showed no overall trend. Figure 1 shows a comparison of droplet spectra and a comparison of parameters is shown in table 1. The error terms represent the short term variability in the data. It is seen that the agreement is good.

Observations of cloud condensation nucleus spectra (CCN) were made just below cloud base using a modified Mee CCN device. Occasional profiles of wind speed and direction at 2m above the local terrain, and of temperature were taken from just below cloud base to the mountain top.

3. ADIABATIC MODEL OF CLOUD DROPLET EVOLUTION

The model described in this section calculates the cloud droplet size distribution of an air parcel subjected to adiabatic ascent. Initially the air has a relative humidity of 99% with a known size distribution of droplets, calculated from the CCN activity spectrum, in vapour equilibrium. We start with a humidity of 99%, since for higher humidities the large nuclei do not have enough time to attain their equilibrium size.

The equations for the model are very similar to those used by Lee and Pruppacher (1977) without entrainment, the only significant difference being that the droplet growth equation has been adapted so that no specific knowledge of aerosol types or mass is required. The equations were integrated numerically using a simple forward difference method.

For droplet growth we have

$$r\frac{dr}{dt} = \frac{S - \frac{A}{r} + \frac{B}{r^3}}{\left[\frac{\rho_w RT}{e(T)D(r)M_w} + \frac{L\rho_w}{K(r)T}\left(\frac{LM_w}{RT} - 1\right)\right]} \qquad (1)$$

where $A = 2M_w\sigma/RT\rho_w$, $B = 3\nu M_w m_s/4\pi\rho_w M_s$, S is the supersaturation, r the droplet radius, M_w and M_s the molecular weights of water and the aerosol, ν the number of ions per aerosol molecule, σ the surface tension of the aqueous solution drop against air, ρ_w the density of water, e(T) the saturation vapour pressure with respect to a flat water surface at temperature T. D(r) and K(r) are (respectively) diffusivity of water vapour and thermal conductivity of air at a drop radius r, L the latent heat of evaporation and R the universal gas constant.

The time variations of the vapour mixing ratio, w_v, and liquid water content, w_L, are given, for adiabatic ascent (no sedimentation) by

$$\frac{dw_v}{dt} = -\frac{dw_L}{dt} \qquad (2)$$

$$\frac{dw_L}{dt} = 4\pi\frac{\rho_w}{\rho_a}\sum r^2 N(r)\frac{dr}{dt} \qquad (3)$$

where ρ_a is the density of air and N(r) the concentration of droos of radius r. The temperature variation is taken to be

$$-\frac{dT}{dt} = \frac{gW}{C_p} + \frac{L}{C_p}\frac{dw_v}{dt} \qquad (4)$$

W is the updraught speed, C_p the specific heat of dry air at constant pressure and g is the acceleration due to gravity. The time variation of supersaturation is

$$\frac{dS}{dt} = \frac{P}{\beta e}\frac{dw_v}{dt} - (1 + S)\left[\frac{\beta L}{R_a T^2}\left(\frac{dT}{dt}\right) + \frac{g}{R_a T} W\right] \qquad (5)$$

where P is the pressure, $\beta = M_w/M_a$ the ratio of the molecular weights of dry air and water, R_a is the specific gas constant of dry air.

Finally the pressure variation is given by

$$\frac{dP}{dt} = -\frac{gPW}{R_a T} \qquad (6)$$

We now show how input data for the model were prepared from the CCN activity spectrum and obtain the required form of the droplet growth equation. The equations of Köhler (Pruppacher and Klett 1978) relate the equilibrium size of a drop with nucleus mass m_s to the ambient supersaturation S.

$$S = \frac{A}{r} - \frac{B}{r^3} \qquad (7)$$

A and B are as previously defined. Differentiation of this equation to find a maximum in S yields a critical radius:

$$r_c = \left(\frac{3B}{A}\right)^{\frac{1}{2}} \qquad (8)$$

Rewriting (7) using (8) we have

$$S = \frac{A}{r} - \frac{1}{3}\frac{r_c^2 A}{r^3} \qquad (9)$$

The Mee activity spectrum gives the number of drops activated at a given supersaturation. We divided the total concentration of drops into categories whose size ΔN_i varies from about $40cm^{-3}$ to $0.05cm^{-3}$ as the drop activation supersaturation (critical supersaturation) decreased. This ensured a small range of critical supersaturations for all drops in each category, and enabled us to assign one value for the critical supersaturation (S_c), to all drops in one category with only small error. It was subsequently found that changing the size of the categories of the CCN caused no significant change in the calculated adiabatic droplet spectrum. For the i^{th} category the critical radius $(r_c)_i$ is related to the assigned critical supersaturation $(S_c)_i$ by setting $r = (r_c)_i$ in equation (9) giving

$$(r_c)_i = \frac{2}{3}\frac{A}{(S_c)_i} \qquad (10)$$

The radius of droplets at cloud base is obtained by substituting the cloud base supersaturation in (9). We assumed a supersaturation $S = -0.01$ giving r_i as a solution of the equation

$$-0.01 = \frac{A}{r_i} - \frac{1}{3}\frac{(r_c)_i^2 . A}{r_i^3} \qquad (11)$$

The input data can now be obtained; for category i we have a drop concentration ΔN_i with critical radius $(r_c)_i$ from (10), and cloud base radius r_i from equation (11).

Finally we rewrite the droplet growth equation using (8) For the category i:

$$r_i \frac{dr_i}{dt} = \frac{S - \frac{A}{r_i} + \frac{A}{3}\frac{(r_c)_i^2}{r_i^3}}{\left[\frac{\rho_w RT}{e(T)D(r)M_w} + \frac{L\rho_w}{K(r)T}\left(\frac{LM_w}{RT} - 1\right)\right]} \qquad (12)$$

We have eliminated S which depends on m_s and can use our knowledge of the critical radius $(r_c)_i$.

Most atmospheric aerosol particles are mixed; i.e. they consist of water soluble and insoluble parts. We have shown in the appendix, that the above equations can still be used for these mixed particles with only very little error.

The updraught speed $W(x)$ of horizontal distance x from the summit was taken to be

$$W(x) = f \, \mathrm{grad}(x) \, U(x) \qquad (13)$$

where $U(x)$ is the local wind at 2 metres above the ground - averaged over about 5 minutes - and estimated from measurements made at different locations up the hill using our instrumented Land Rover, $\mathrm{grad}(x)$ is the local gradient estimated from a map scale (1:25,000), and f is a factor introduced to allow for the retarding effect of friction at the ground. Assuming an approximately logarithmic wind profile we took f = 1.5. Subsequent analysis using the linear theory for turbulent flow over a hill (Jackson and Hunt 1975) suggests this to be a reasonable estimate. Values of temperature and pressure required for the calculations were measured at cloud base.

4. DROPLET LOSS TO GROUND

The effect of loss of drops to ground by eddy diffusion and gravitational sedimentation was investigated using the equation

$$\frac{\partial N(r)}{\partial t} = \frac{\partial}{\partial z}\left(K(z)\frac{\partial N(r)}{\partial z}\right) + V_r\frac{\partial N(r)}{\partial z} \qquad (14)$$

where $N(r)$ is the drop concentration of radius r, V_r is the terminal velocity and $K(z)$ is the eddy diffusivity at height z. The equation was solved numerically using a forward difference method and starting with a typical drop size distribution which was the same throughout the cloud. The integration was carried out for the time it takes a parcel of air to travel from the cloud base to the mountain top.

The primary difficulty in carrying out these calculations is in the choice of the eddy diffusivity, K. We used

$$K(z) = 0.4zu_* \quad z \leq 150m$$
$$K(z) = 60\ u_* \quad z > 150m \qquad (15)$$

where u_* is the friction velocity deduced from 2m and 10m winds at mountain top. The first expression for K is based on the assumption of near neutral stability, and the second simulates a highly diffusive outer layer. This is certainly a large overestimate for any situation in which mechanical turbulence is dominant (eg. Bradley 1980). Convection and the occurrence of rotary type motions may both act to increase deposition; however no information is available on the magnitude of these effects. It is felt that the above eddy diffusivity will still lead to an upper boun for droplet loss to ground. For the upper boundary condition K was assumed to fall rapidly to zero at cloud top, i.e. at the base of the capping inversion. Support for this notion comes from turbulence structure observations in the vicinity of inversions over level country (e.g. Caughey and Palmer 1979) and from the appearance of an echo free region, implying small turbulence levels, above the inversion in the acoustic records

The results showed that depletion was only significant for clouds of vertical depth $\leq$ 200m. The cloud depth is a minimum above the mountain-top. We estimate the depth to be greater than 500m, between 50 and 100m, and around 300m for the cases I, II and III respectively. Hence absolute values of drop concentration and liquid water content must be treated with some caution, especially in case II, where subadiabatic liquid water contents may not be due to entrainment alone. The preferential deposition of larger drops by gravitational sedimentation was negligible for a typical range of drop sizes, and caused no significant change in the drop size distribution in the time required for the cloud to flow from cloud base to the mountain top.

5. THE FIELD EXPERIMENTS

Case I 10 May 1979

A deep isolated cap cloud was located over the ridge at GDF and precipitation was falling into it from an initially much higher deck of altostratus associated with an approaching warm front. Winds were south easterly, about 10m s^{-1} at 10m above the summit. A section of the acoustic record for the period ~11.30 to 12.10 BST is given in Figure (2). This illustrates the presence of fairly weak thermal plumes extending up to ~50-100m in height from the hill top. It is also apparent, from the absence of an elevated layer echo, that no significant entrainment interface existed within the lowest 300m, and this tends to support the view that on this occasion entrainment effects at the mountain-top were likely to be quite small. (The thin stationary echo at ~80m is from one of the communication towers on GDF.) Figure 3a shows that after the formation period the cloud had an approximately adiabatic liquid water content. (The adiabatic λ value was calculated from the height and temperature of cloud base using the model.) Figure 3b shows the variation in 15 minute averages of the drop concentration and P the percentage of 3-second drop counts which satisfy one of the conditions

$$N > \bar{N} + 2\sqrt{\bar{N}}$$

or

$$N < \bar{N} - 2\sqrt{\bar{N}} \qquad (16)$$

as a measure of the small scale inhomogeneity in the cloud, as used by Blyth et al (1980). N is the number of drops in the 3-second histogram and $\bar{N}$ is the 15 minute average drop concentration. Care was taken to establish that the number of histograms satisfying one of the criteria (16) was not significantly affected by trends in the mean drop concentration over a 15 minute period. The low values of P indicate a fairly homogeneous cloud structure.

Figure 4 shows a typical spectrum in the cloud, and the adiabatic model spectrum calculated for the same time.

Figure 3 and 4 strongly suggest a cloud with near adiabatic properties, whose nearly homogeneous structure indicates little effect from interaction with its environment. Examination of anemograph records from the mountain top shows that the air was at least as turbulent in case study I as in cases II and III. It is therefore reassuring for the interpretation of cases II and III that P is small, indicating that water loss to ground is not introducing structure into the cloud on the scales examined.

The rainfall rate in the area of GDF did not exceed 2mm hr^{-1} and rough calculations confirm that the effect of scavenging of droplets by precipitation, or the breakup of rain drops had a negligible effect on the droplet spectra.

Case II 14 May 1979

The cap cloud formed in a weakly convective boundary layer capped by a strong subsidence inversion; routine ascents showed that this was generally at around 600m above lowland areas, but it was forced to rise in the vicinity of the hill, and was observed by the acoustic sounder to be between 10m and 100m above the mountain top. Cloud base was 600m below the mountain top at 07.00 BST and thereafter rose steadily to be 150 below the summit at 15.00 BST. The 10m wind at the summit was from 210^{o} with a speed of ~10m s^{-1}. Figure (5) presents a section of the acoustic recording between 1030 and 1120 BST. The very dark elevated layer echo which varies in height from ~10m to above 100m is from the subsidence inversion. Undulations were present on a range of scales, i.e. from a few hundred metres to mesoscale variations of ~10-15km (e.g. the dip which occurs between 10.40

and 11.00 BST. The dark region extending from the inversion into the near surface region probably represents entrained air mixing into the boundary layer. Thus, whilst entrainment was almost certainly occurring locally the intensity of the echo from the inversion (reflecting the inversion strength) suggests that it would be weak. The sounder also indicates the presence of weak convection under the inversion. The CCN distribution was much more maritime than in either case I or case III. Curve P of Figure 6 shows the percentage of 3-second drop counts which satisfy the criterion (16). Although the mean liquid water content was substantially subadiabatic, especially early in the period,(see Figure 7, which shows 15 minute averages of liquid water content), the regions of highest drop counts had liquid water contents which approached the adiabatic value estimated from the observations of cloud base height, and drop concentrations similar to those predicted by the model. However the measured concentrations must be treated with caution in view of the adjustment described earlier. Further the droplet spectrum observed for these regions agrees quite well with the calculated adiabatic spectrum, especially early in the day as can be seen from Figure 8. The spectra in the high and low drop concentration regions (defined by (16)) are shown in Figure 9. The shapes of the spectra, taken with the proximity of the dry air source, suggest that the inhomogeneities in the cloud were produced by the entrainment of undersaturated air, and this is supported by the acoustic sounder trace, (Figure 5).

The turbulent mixing model outlined by Baker and Latham (1981) was utilised to predict changes to the high concentration spectrum (A) in Figure 9 resulting from the mixing-in of environmental air. A specific test was to see whether the low concentration spectrum (B) was reproduced. The ranges of input

parameters utilised in these calculations, based on the meteorological observations, were: ϵ, (the turbulent energy dissipation rate), 2×10^{-3} to 2×10^{-2} $m^2 s^{-3}$, estimated from the mean wind-speed at an altitude of 10m, the assumption of neutral stability and an assumed surface roughness of 2cm; and λ (the radius of the spherical entrained blob) = 50 to 100m, estimated from the acoustic sounder traces. We assumed that the supersaturation S, estimated from ascent data, was around -0.2, $m_s = 10^{-15}$g, and that the temperatures before mixing of the cloudy and environmental air, T_c and T_e, were 6C (measured) and 8C (estimated) respectively. The spectrum A ($L = 0.45g\ m^{-3}$) was subdivided into 5 size-categories.

Curve C in Figure 9 is calculated on the basis of this mixing model, and is seen to be in close agreement with the observed spectrum B, which has a reduced liquid water content of $0.08g\ m^{-3}$. As the mixing process proceeds, in the calculations, there are many regions, at particular times, where $L = 0.8g\ m^{-3}$, but examination shows that the droplet spectra are always similar to C. It was found also that this spectrum was insensitive to reasonable variations in the input parameters (Baker and Latham, 1981). This agreement between observed and calculated spectra encourages us to believe that the mixing model is capable of describing, with adequate precision, the influence of entrainment upon the droplet spectra.

Examination of curve P, Figure 6, shows that there is an entrainment maximum around 11.00 after which a continual decrease occurs until near the end of the period. Despite this the low count/high count spectra showed that the form of the mixing remained as described above. The inhomogeneity at the end of the period was due to patchy cloud as the base rose above the mountain top.

The large rise in drop concentrations towards the end of the period was partially reproduced by the adiabatic model. The increase in the calculated value of N was due to higher updraught speeds near cloud base as this moved up the hill. This produced higher peak supersaturations and so activated more nuclei. However the narrowing of the spectrum was greater than predicted. This may be a consequence of the crudity of the model but would result from a change to a more continental CCN. Measurements with the Mee device were unavailable to test this latter possibility, but a change to a more continental CCN had occurred by the next day.

Case III 15 May 1979

The day was characterised by light SW winds, (less than 4m s^{-1} at the mountain top). A general cover of stratus and stratocumulus cloud enveloped the mountain. At 11.00 BST cloud base was 500m below mountain top and rose to first clear the mountain at 1400 BST. There was a weak subsidence inversion (much weaker than in case II) about 150m above the mountain top. This was clearly revealed in the acoustic sounder record, a section of which is given in Figure (10). The important features to note are that the echo layer is much weaker than on the 14th and is also highly contorted on a range of scales. Convection beneath the interface is also much stronger than on the previous day. These features suggest a situation in which entrainment effects are likely to be prominent. Regions of entraining air can be seen extending from the interface to near the ground at ~14.10 BST and again at ~14.20 BST.

During the period up to 14.30 the adiabatic liquid water content fell as cloud base rose (Figure 11), although initially the observed liquid water content and drop concentrations both

...e presumably due to increasing convective activity and upward transport of moisture and CCN in the boundary layer. After 12.00 the acoustic sounder showed entrainment into the cloud through the capping inversion on scales of several tens of metres, (Figure 10). A large fall in mean drop count occurred as the cloud became very inhomogeneous, as shown in Figure (12), but the peak drop concentrations observed in the patches of thickest cloud remained unchanged until about 13.10. During this time the high and low count spectra (derived by the criteria 16) became very similar in shape (Figure 13A,B) suggesting that the mixing was extremely inhomogeneous. Within this period the observed spectrum became appreciably broader, (Figure 14,A). However, it was no broader than the model adiabatic spectrum calculated for the same time using CCN measurements made at 11.40. Curve C in Figure 13 is the spectrum predicted from the turbulent mixing model for input parameters estimated from the meteorological measurements in the same manner as for Figure 9. Their values were: $\epsilon = 5 \times 10^{-4} m^2 s^{-3}$, $\lambda = 50m$, $S = -0.2$, $T_c = 8^oC$, $T_e = 5^oC$. The initial spectrum A, ($L = 0.24g\ m^{-3}$) was subdivided into 12 size-categories. There is seen to be good agreement between the observed and calculated spectra, B and C respectively.

During the remainder of the experiment cloud base remained near the mountain top. The curve of the number of histograms outside the 2 N criterion shows a marked lull in mixing around 16.10 BST. This was confirmed by the acoustic sounder. This period was characterised by a narrower spectrum as shown in Figure 14(B). These experiments therefore provide further strong evidence for the importance of understanding the nature of the entrainment processes in any study of the microphysical development of real clouds.

6. DISCUSSION

The general conclusions from these three case studies may be interpreted in terms of the recently developed ideas on the interaction of clouds with their environment (Baker et al, 1980). For extreme inhomogeneous mixing the time constants for eddy dissipation and droplet evaporation, $\tau_T/\tau_E \rightarrow \infty$, whereas for classical mixing $\tau_T/\tau_E \rightarrow 0$.

In case I local turbulence levels were high, but the cloud was deep and exhibited an approximately adiabatic structure. Any entrainment effects produced small changes at the hilltop sampling point. We may estimate the relative extents to which the entrainment/mixing processes in cases II and III are inhomogeneous by considering the ratio $(\tau_T/\tau_E)_{III}/(\tau_T/\tau_E)_{II}$. Ignoring the contribution to the turbulence kinetic energy budget from buoyancy production we assume that most of the turbulence energy is generated through mechanical production. The above ratio can then be written as follows:

$$\frac{(\tau_T/\tau_E)_{III}}{(\tau_T/\tau_E)_{II}} \approx \frac{(\lambda^2/\epsilon)^{\frac{1}{3}}_{III}}{(\lambda^2/\epsilon)^{\frac{1}{3}}_{II}} \times \frac{(r^2 + 2ar)_{II}}{(r^2 + 2ar)_{III}} \times \frac{S_{III}}{S_{II}} \quad (25)$$

where λ is a length scale taken to be characteristic of both the sizes of the entrained volume of air and the turbulent mixing lengths, a ($\sim 5\mu m$) the scale length associated with the condensation coefficient and S the undersaturation of the entrained air. The acoustic sounder traces indicate that $\lambda_{III}/\lambda_{II} \sim 1$, the droplet data show that $r_{II} \sim 12\mu m$, $r_{III} \sim 6\mu m$, and we employ the values of ϵ and S presented earlier: $\epsilon_{II}/\epsilon_{III} \sim 4$ to 40, $S_{II}/S_{III} \sim 1$. It therefore follows that

$$\frac{(\tau_T/\tau_E)_{III}}{(\tau_T/\tau_E)_{II}} \sim 4 \text{ to } 40$$

Buoyancy production, as indicated by the acoustic sounder, was certainly much larger during case III than case II and would therefore have acted to reduce the above ratio. However, inclusion of this factor would not be expected to alter the conclusion that the above ratio is consistent with the experimental observations that the cloud is much more inhomogeneous in case III than in case II.

A further prediction of the inhomogeneous mixing model of Baker et al (1980) is that the drop concentrations of the largest drops are greater than those obtained by purely adiabatic growth. Comparisons of calculated adiabatic spectra and observed mean spectra show no clear evidence for this (the inaccuracies in the calculated updraught profiles do not seriously affect this result since the measured CCN distribution leads to calculated spectra much more similar in shape to the broadest rather than the narrowest observed spectra for a range of likely updraughts). In case II the lack of broadening can be explained if entrainment effects are confined close to the region near the mountain top where the wind shear across the inversion interface is greatest; droplets unaffected by the entrained air will not now have time to grow to sizes which are significantly in excess of those resulting from adiabatic growth. In case III we observed that the highest concentrations of large drops occurred in regions where the degree of inhomogeneity and the liquid water content were highest.

APPENDIX

THE EFFECT OF MIXED NUCLEI ON THE DROPLET GROWTH EQUATION

It is assumed that the water insoluble part is a sphere of radius x. The Kohler equation for the equilibrium drop size is (Pruppacher and Klett, 1978)

$$S = \frac{A}{r} - \frac{B}{r^3 - x^3} \qquad (A1)$$

where A and B are as defined in the body of the paper. Differentiating as before gives

$$B = \frac{(r_c^3 - x^3)^2 A}{3r_c^4} \qquad (A2)$$

and rewriting (A1)

$$S = \frac{A}{r} - \frac{(r_c^3 - x^3)^2}{(r^3 - x^3)} \cdot \frac{A}{3r_c^4} \qquad (A3)$$

Setting $r = r_c$ the critical radius is related to the critical supersaturation by

$$r_c = \frac{2}{3} \frac{A}{S_c}\left(1 + \frac{x^3}{2r_c^3}\right) \qquad (A4)$$

This equation is identical to (10) for completely soluble aerosol if $(x^3/2r_c^3) \ll 1$

Pruppacher and Klett(1978), table 6.3, present some values related to this parameter. They use salt and silicon dioxide respectively as the soluble and insoluble parts. With these compounds the error is less than 3% for $m_x/m_n < 0.9$ and $m_N > 10^{-15}$g, where m_x is the mass of the insoluble part and m_N the total nuclear mass. Work by Hänel (1976) has shown that all CCN likely to be activated at Great Dun Fell satisfy these conditions well.

For the equilibrium drop radius r at cloud base we have

$$-0.01 = \frac{A}{r} - \frac{(r_c^3 - x^3)^2}{(r^3 - x^3)} \frac{A}{3r_c^4} \qquad (A5)$$

$$= \frac{A}{r} - \frac{r_c^2 A}{3r^3} \left(1 - \left(\frac{x}{r_c}\right)^3\right)^2 \left(1 - \left(\frac{x}{r}\right)^3\right)^{-1} \qquad (A6)$$

If we can assume $\left(\frac{x}{r_c}\right)^6$, $\left(\frac{x}{r}\right)^6 \ll 1$, we can use first order approximations to obtain

$$-0.01 = \frac{A}{r} - \frac{r_c^2 A}{3r^3} \left[1 - 2\left(\frac{x}{r_c}\right)^3 + \left(\frac{x}{r}\right)^3\right] \qquad (A7)$$

This equation is identical to (11) if we let $(r_c)_{mixed} = (r_c)_{soluble}$ which introduces only small error as above and if $\left(\frac{x}{r}\right)^3 - 2\left(\frac{x}{r_c}\right)^3 \ll 1$. $\left(\frac{x}{r_c}\right)^3$ is small as before so we need $\left(\frac{x}{r}\right)^3 \ll 1$.

For the smallest particles where the error is greatest $r \approx \frac{r_c}{3}$; thus $(x/r)^3 \sim 1$ (Pruppacher and Klett, table 6.3). There is therefore considerable error in the cloud base radius calculated for these small particles if they have a very large insoluble fraction. However, this will not introduce significant inaccuracies to the droplet spectrum calculated in the cloud , since these small particles have small critical radii and when they reach these radii the error is small, as previously shown. For other particles the error is small throughout growth.

TABLE 1

Parameter \ Sensor	ASSP-100	K.P.
$\bar{r}$ (μm)	5.6 $\pm$ 0.1	5.6 $\pm$ 0.1
N (cm^{-3})	230 $\pm$ 20	255 $\pm$ 20
L ($g\ m^{-3}$)	0.23 $\pm$ 0.03	0.22 $\pm$ 0.03

Comparison of mean drop radius $\bar{r}$, drop concentration N, and liquid water content L, for PMS ASSP and Daily Probe device : Case III, 15 May 1979, 1635 - 1650 hours.

REFERENCES

Baker M B and Latham J	1979	"The evolution of droplet spectra and the rate of production of embryonic raindrops in small cumulus clouds" J.Atmos.Sci., 36, 1612-1615
Baker, M B, Corbin R G and Latham J	1980	"The influence of entrainment on the evolution of cloud droplet spectra: I A model of inhomogeneous mixing" Quart J. Roy.Met.Soc., 106, 581-598
Blyth A M, Choularton T W, Fullarton G, Latham J, Mill C S, Smith M H and Stromberg I M	1980	"The influence of entrainment of the evolution of cloud droplet spectra: II Field experiments at Great Dun Fell" Quart. J. Roy.Met.Soc., 106, 821-840
Bradley E F	1980	"An experimental study of the profiles of wind speed, shearing stress and turbulence at the crest of a large hill" Ibid, 106, 101-123
Caughey S J, Crease B A and Roach W T	1981	"A field study of nocturnal stratocumulus. II. Turbulence structure and entrainment" submitted to Quart J Roy Met Soc
Caughey S J, Dare W M and Crease B A	1978	"Acoustic sounding of radiation fog" Met Mag., 107, 103-113
Caughey S J and Palmer S	1979	"Some aspects of turbulence structure through the depth of the convective boundary layer" Quart J Roy Met Soc, 105 811-827
Conway B J, Caughey S J, Bentley A N and Tufton J D	1981	"Ground based and airborne holography of ice and water clouds" Atmos. Environ (submitted)
Conway B J	1980	

Corbin R G, Latham J, Mill C S, and Stromberg I M 1978 "An assessment of the Keily Probe for the ground based measurement of drop size distributions in clouds" Quart J Roy Met Soc., 104, 729-736

Jackson P S and Hunt J C R 1975 "Turbulent wind flow over a low hill" Ibid, 101, 929-955

Kitchen M 1979 "A comparison of measurements of cloud liquid water content in stratocumulus between a Knollenberg Axially Scattering Spectrometer probe and a Johnson-Williams hot wire instrument" MoD (Air Force Dept) Met Research Committee Paper MRCP-467.

Lee I Y and Pruppacher H R 1977 "A comparative study of the growth of clouds by condensation using an air parcel model with and without entrainment" Pageoph, 115, 523-545

Moulsley T J and Cole R S 1979 "High frequency acoustic sounders" Atmos. Envir., 13, 347-350

Pruppacher H R and Klett J D 1978 Microphysics of Clouds and Precipitation D Reidel (pub)

Ryder P 1976 "The measurement of cloud droplet spectra" Int. Conf. Cloyd Phys., Boulder, Colorado 576-580

Slingo A, Brown R and Wrench C L 1981 "A field study of nocturnal stratocumulus: III. High resolution radiative and microphysical observations" submitted Quart J Roy Met Soc

LEGENDS TO FIGURES

Figure 1 Measured size distribution on 15th May 1979 for the period 1635-1650. (A) Keily probe, (B) ASSP.

Figure 2 Case I; Acoustic sounder trace. Dark regions represent echoes from thermal plumes.

Figure 3a Case I. Observed (A) and calculated (B) liquid water contents L.

Figure 3b Drop concentration N and percentage P of histograms outside $\overline{N} \pm 2\sqrt{\overline{N}}$ during the period covered by case I.

Figure 4 Case I. A, observed size distribution over the period 1331 to 1346 BST using the KP. $\overline{N}$ = 265 cm^{-3}, L = 0.28 gm^{-3}. B, calculated spectrum N = 380 cm^{-3}, L = 0.31 gm^{-3}.

Figure 5 Case II; Acoustic sounder trace. The intense layer-echo at around 50-100m represents the base of the inversion or entrainment interface.

Figure 6 Drop concentration N, percentage P of histograms outside $\overline{N} \pm 2\sqrt{\overline{N}}$, and mean radius $\overline{r}$ during the period covered by case II

Figure 7 Observed (A) and calculated adiabatic (B) liquid water contents L during period covered by case II.

Figure 8 Case II. A, measured size distributions for the period 0830 to 0845 BST. $\overline{N}$ = 132 cm^{-3}, B, calculated adiabatic spectrum N = 212 cm^{-3}.

Figure 9 Case II. Size distributions. A, observed high count spectrum, B, observed low count spectrum. A,B, averaged over 15 minute period 0800-0815 BST. C, calculated on the turbulent mixing model of Baker and Latham (1981) for parameter values given in the text. A, L = 0.49 m^{-3}: B,C, L = 0.09 m^{-3}.

Figure 10 Case III, acoustic sounder trace

Figure 11 Observed (A) and calculated (B) liquid water contents during the period covered by case III.

Figure 12 Drop concentration N, percentage P of histograms outside $\overline{N} \pm 2\sqrt{\overline{N}}$, and mean radius $\overline{r}$ during the period covered by case III.

Figure 13 Case III. Measured size distributions for the period 1236-1251 BST. A, high count spectrum. B, low count spectrum. C, calculated on the turbulent mixing model of Baker and Latham (1981) for parameter values mentioned in the text. A, $L = 0.24 g\ m^{-3}$: B,C, $L = 0.14 g\ m^{-3}$.

Figure 14 Case III. A, measured size distributions for the period 1257-1306 BST. $\overline{N} = 258\ cm^{-3}$, $\overline{L} = 0.47\ gm^{-3}$ B, measured size distributions for the period 1622-1637 BST. $\overline{N} = 256\ cm^{-3}$, $L = 0.20\ gm^{-3}$

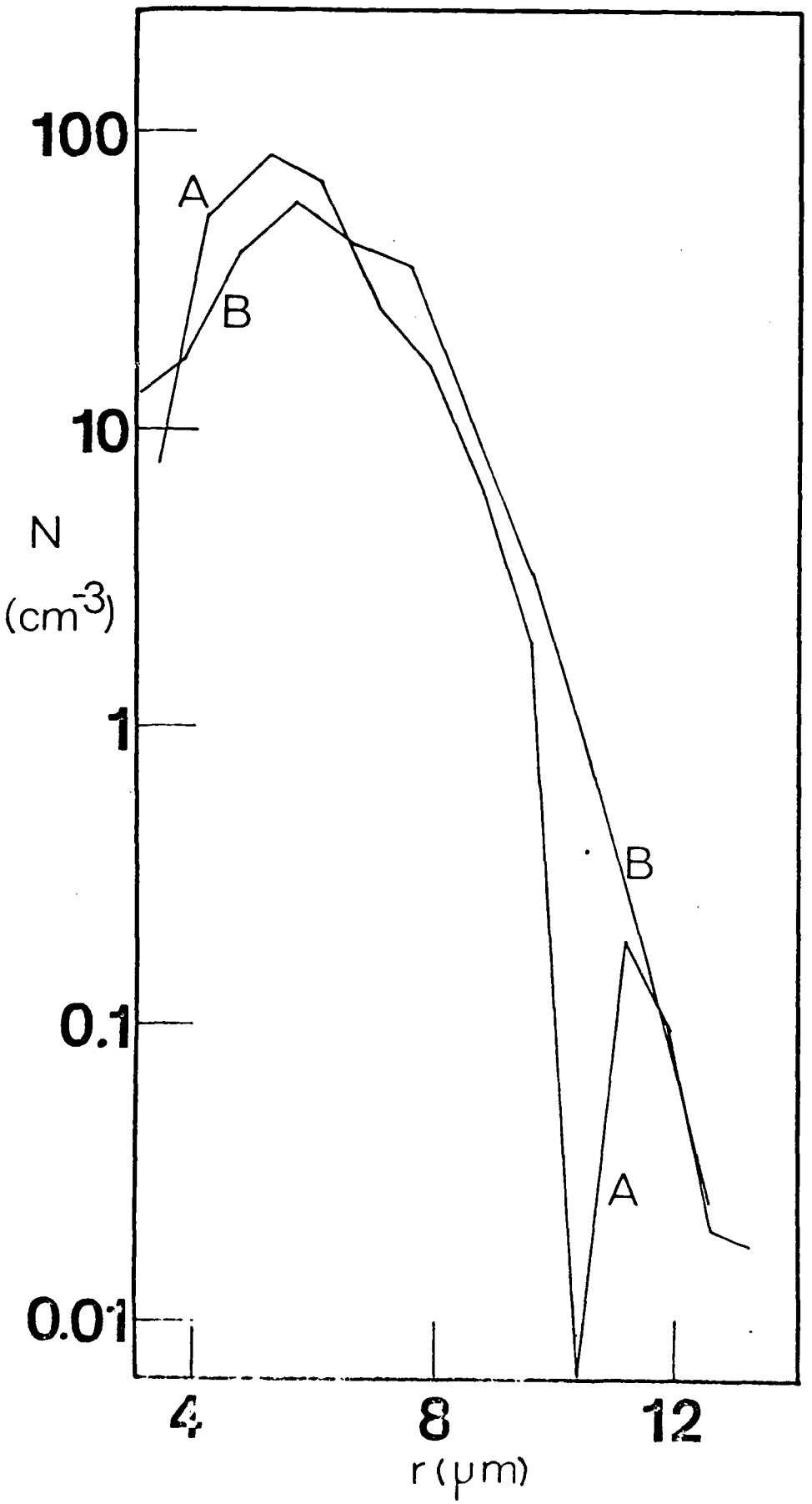

Figure 1

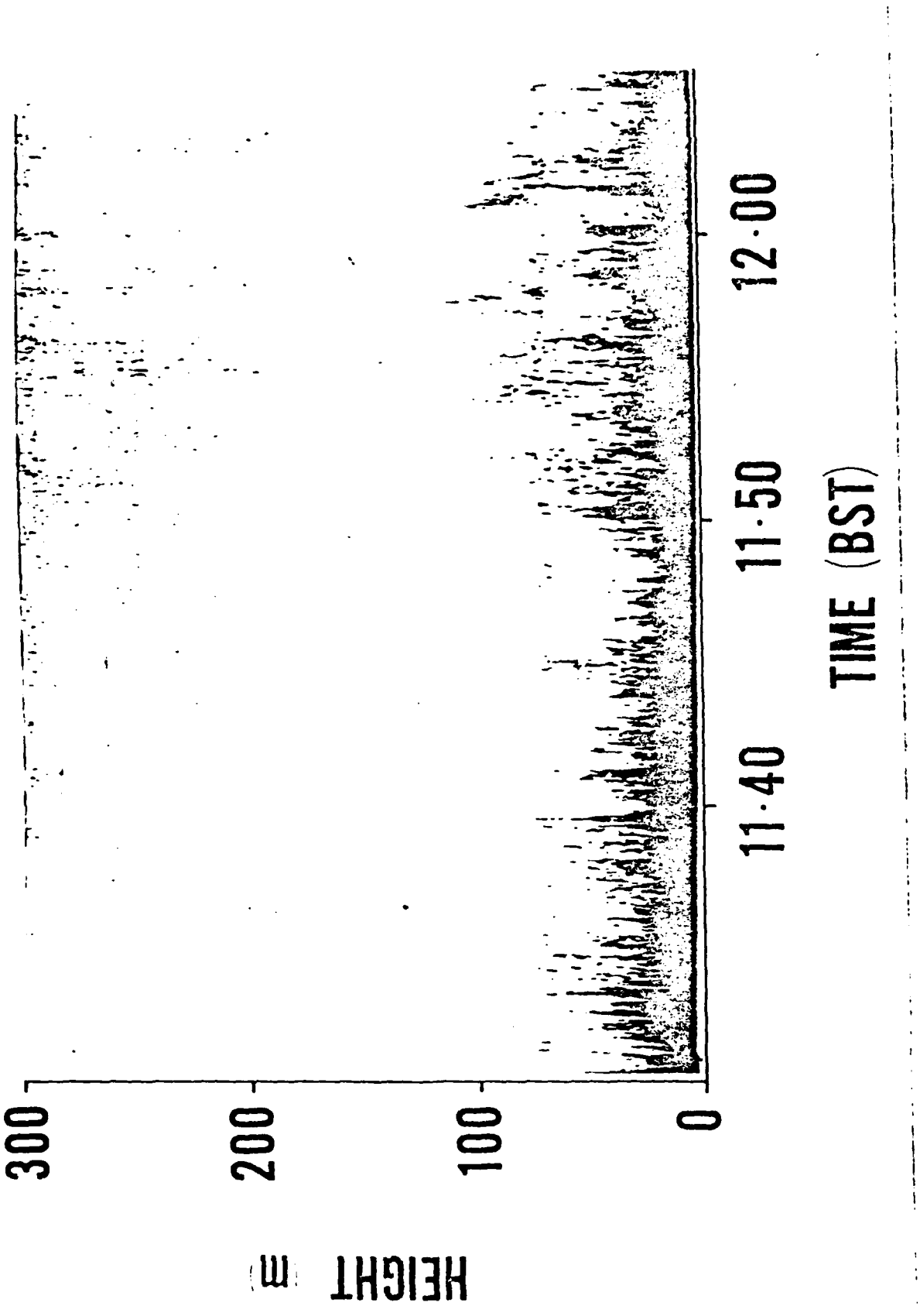

Figure 2

Figure 3

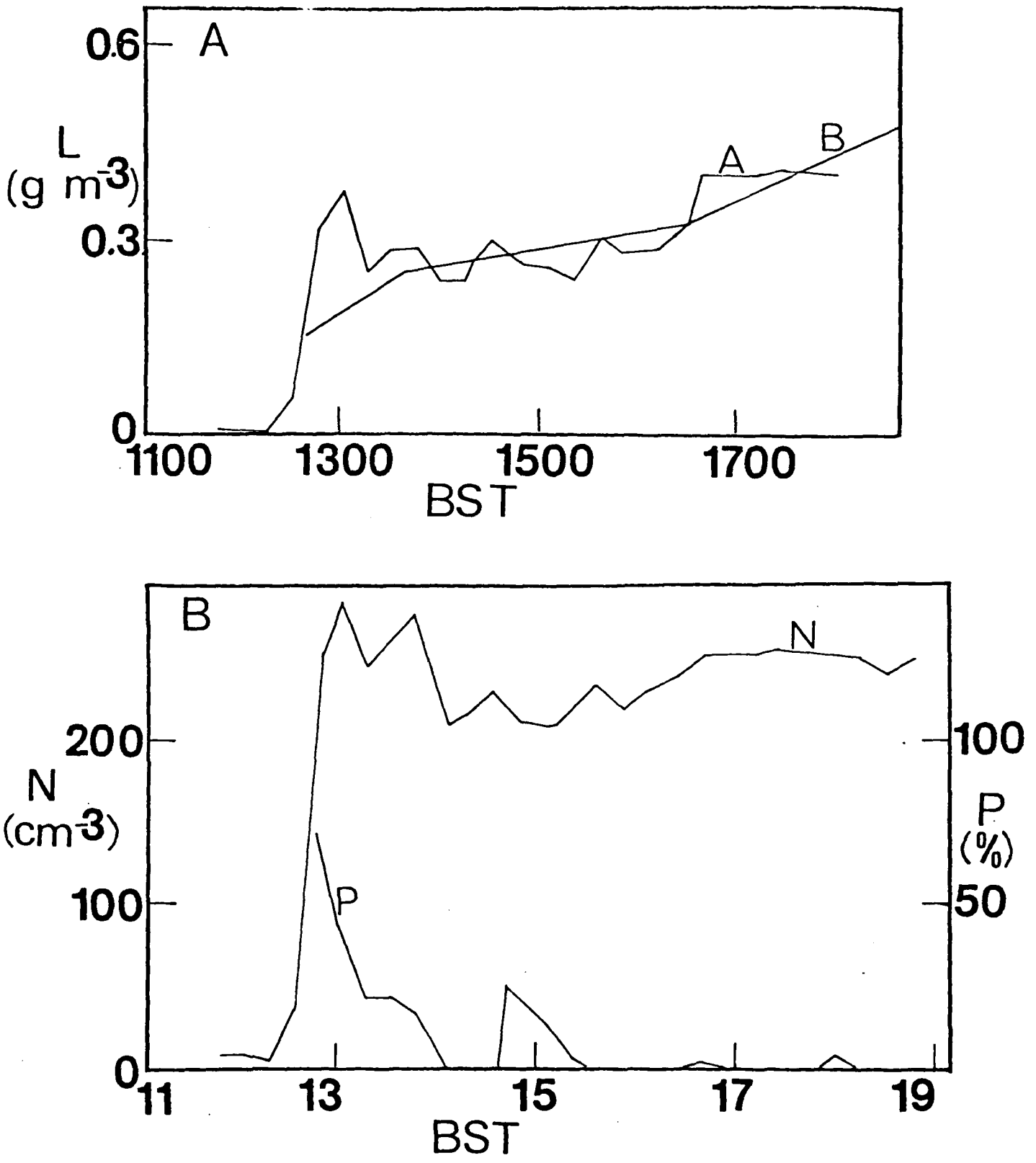
A
0.6
0.3
0
L
(g m-3)
A
B
1100
1300
1500
1700
BST
B
200
100
0
N
(cm-3)
P
100
50
P
(%)
N
11
13
15
17
19
BST

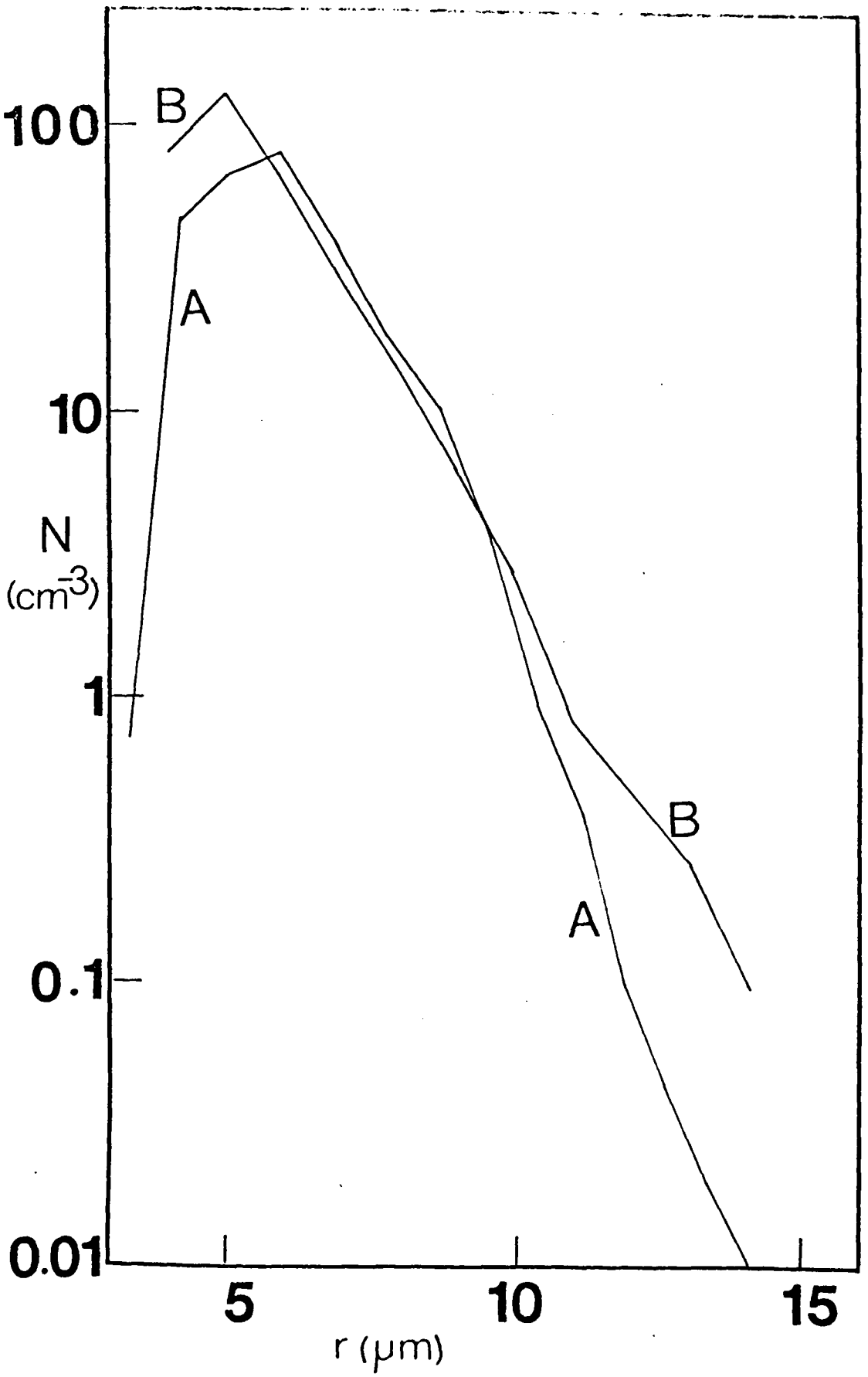

Figure 4

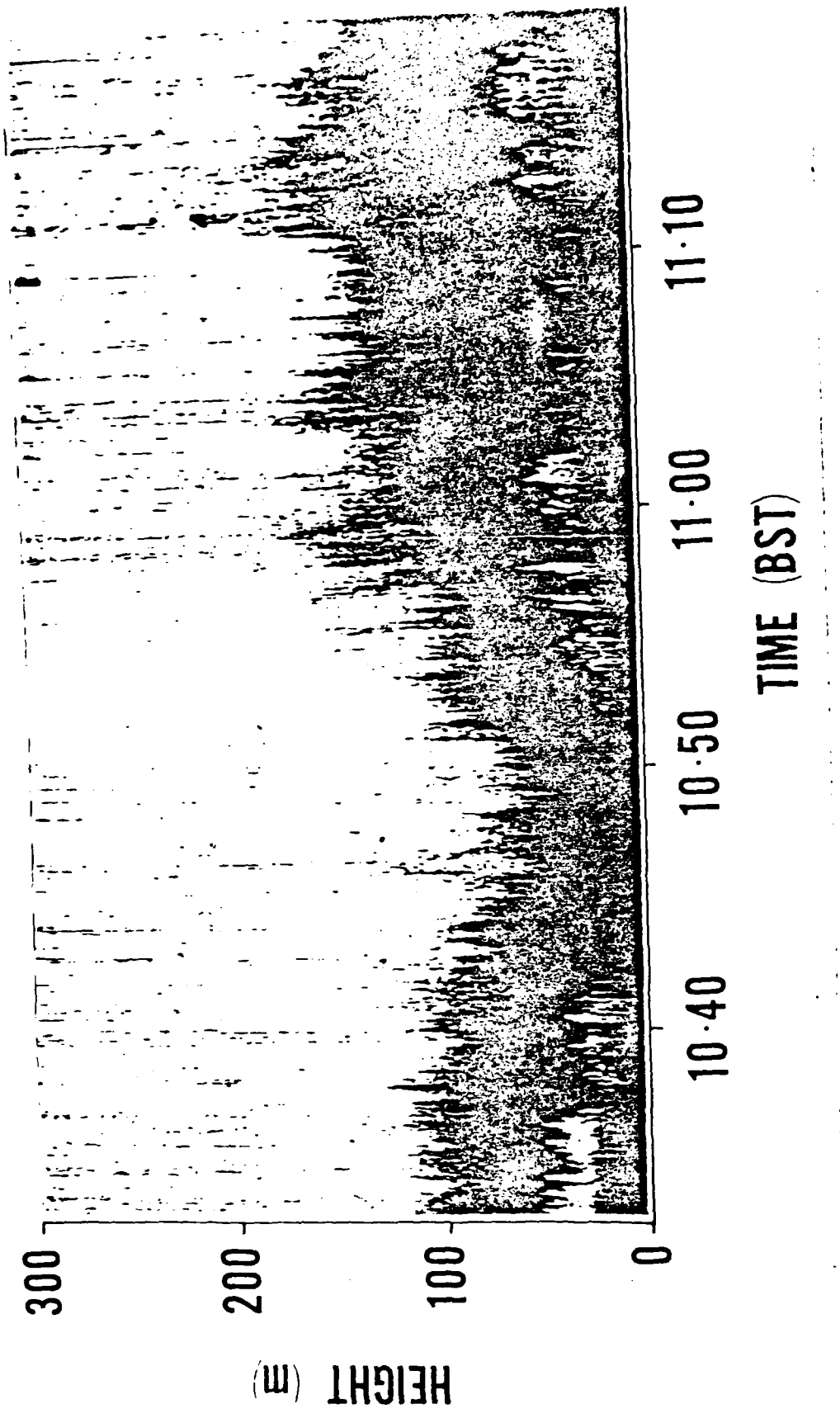

Figure 5

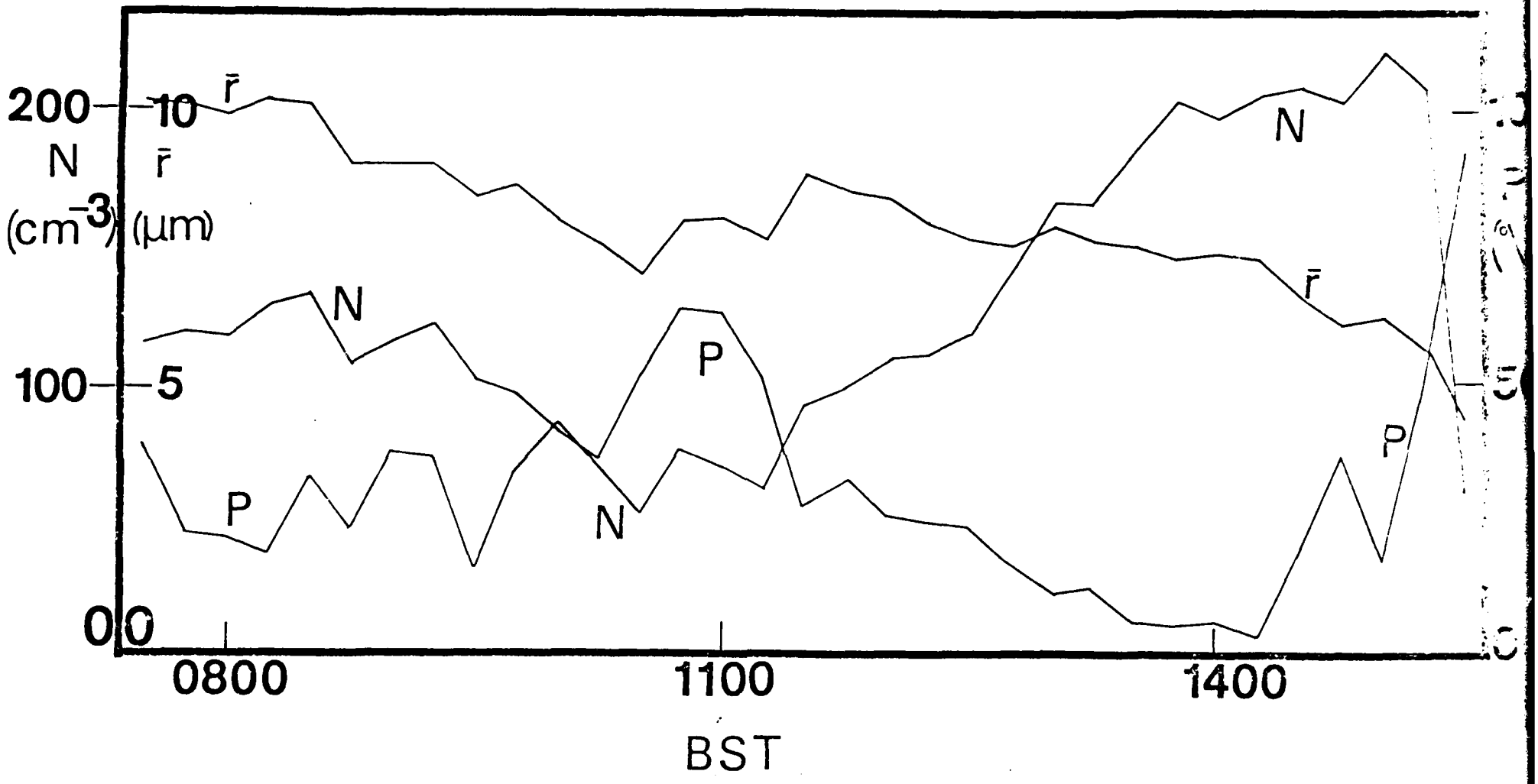
200
10
$\bar{r}$
N
$\bar{r}$
(cm^{-3})
(μm)
N
P
N
P
N
$\bar{r}$
P
100
5
0
0
0800
1100
1400
BST

Figure 6

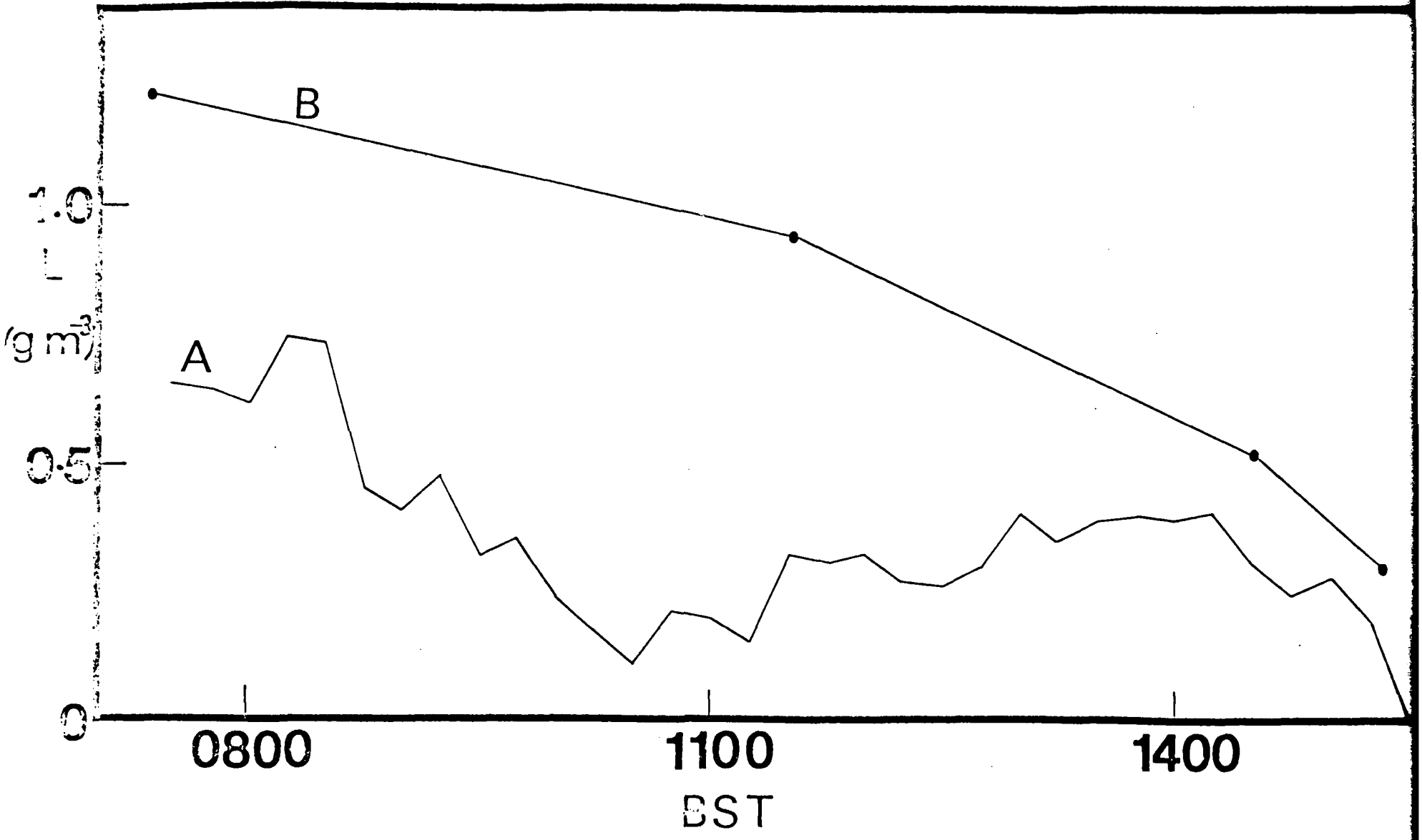

Figure 7

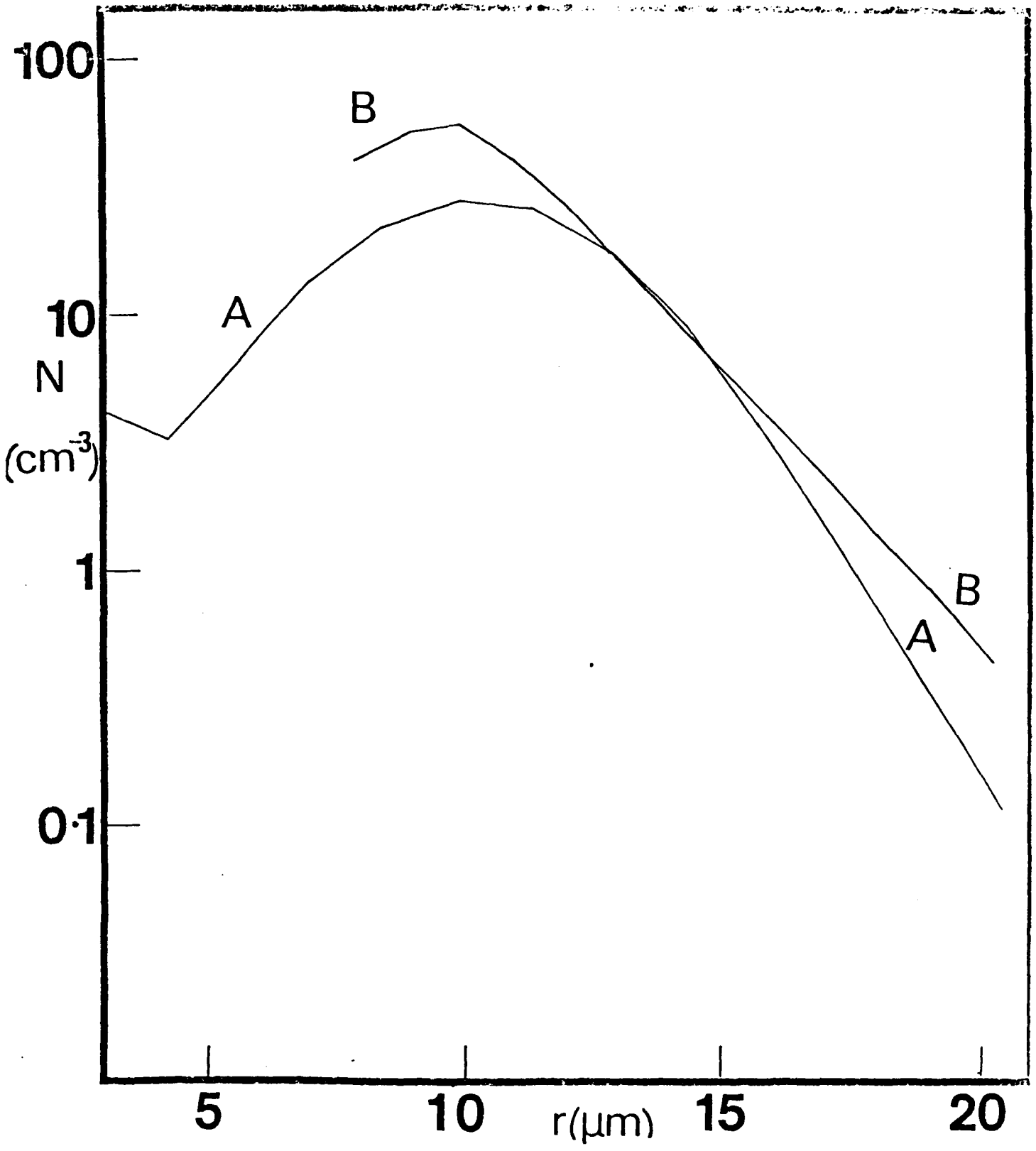

Figure 8

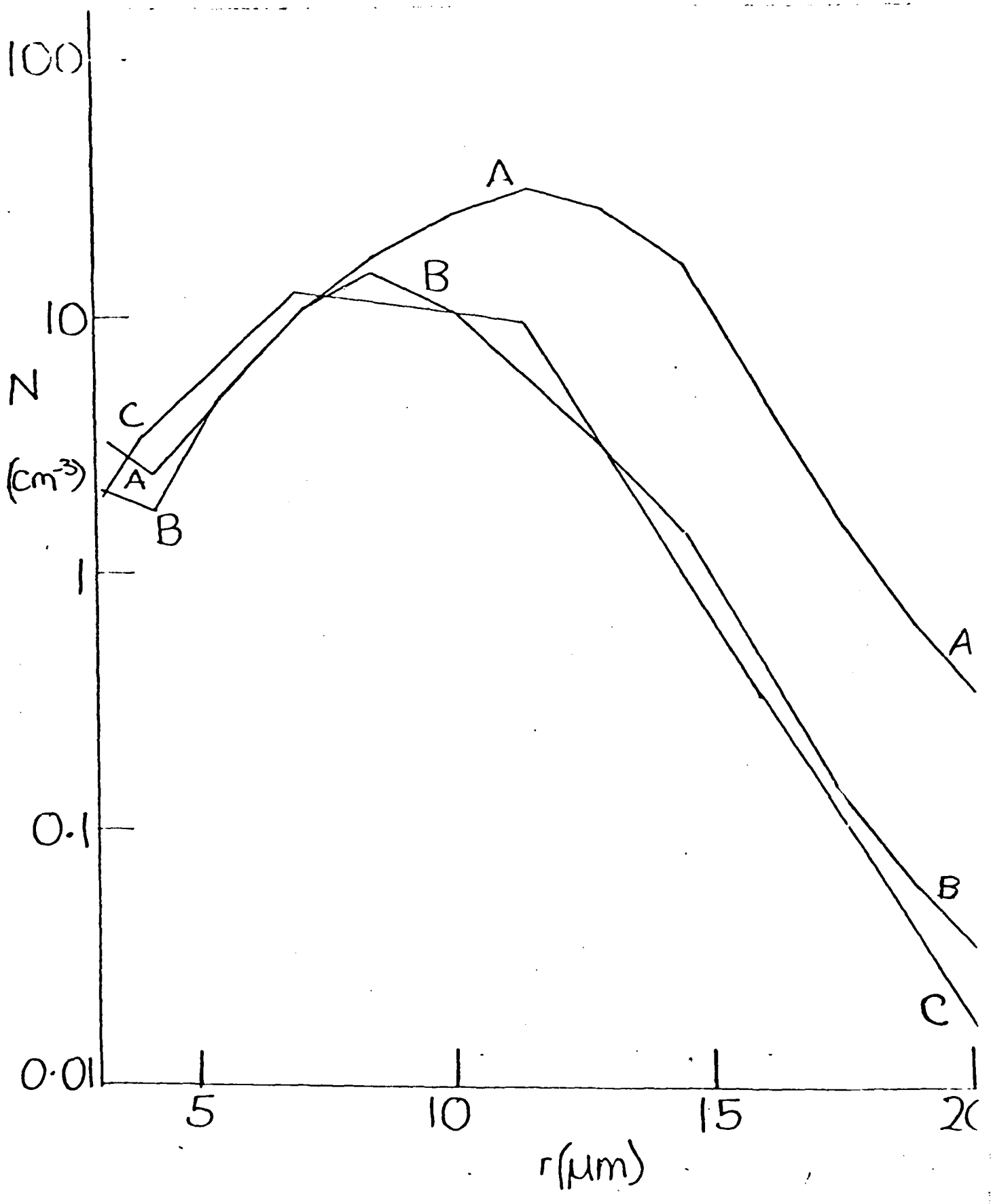

Figure 9

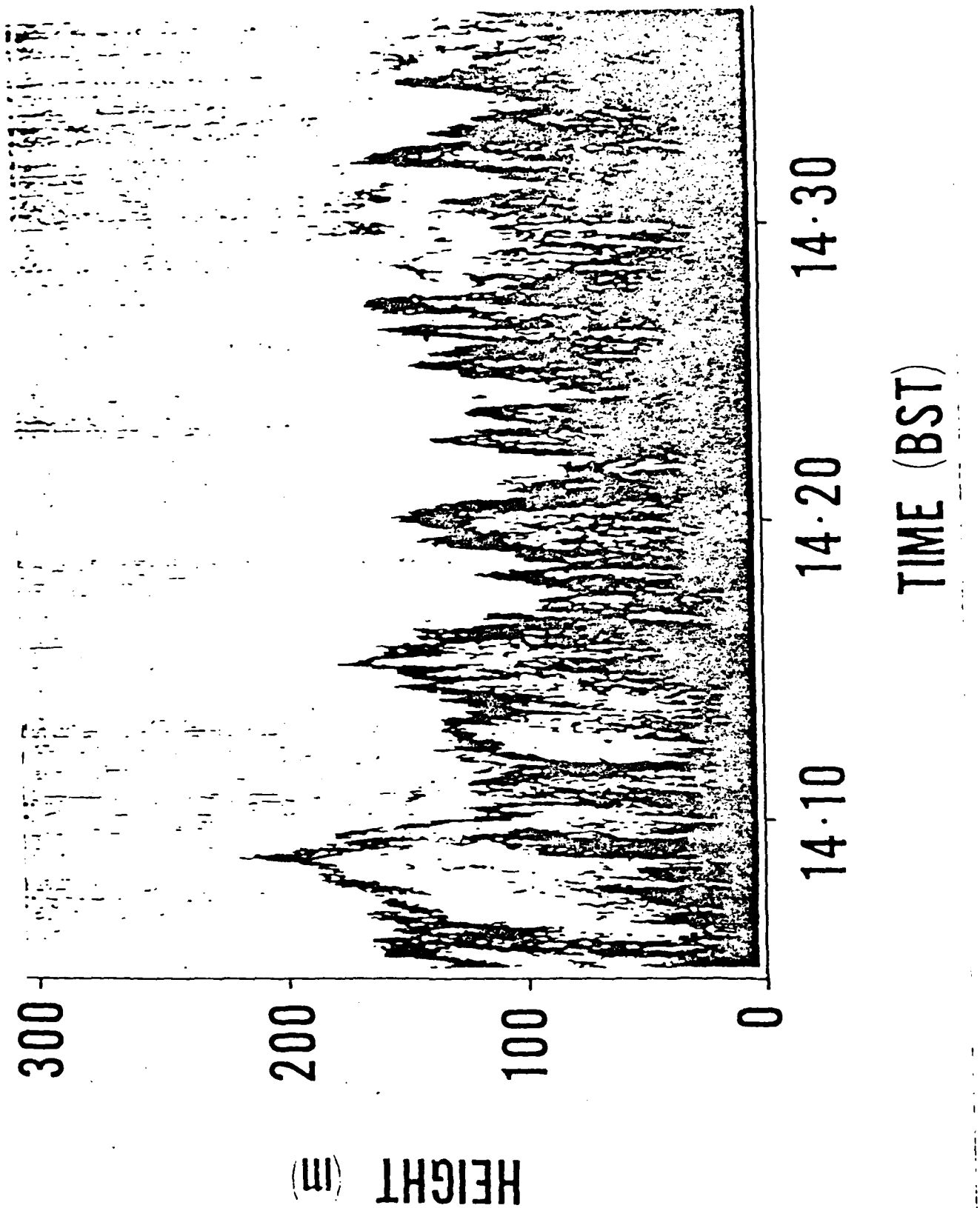

Figure 10

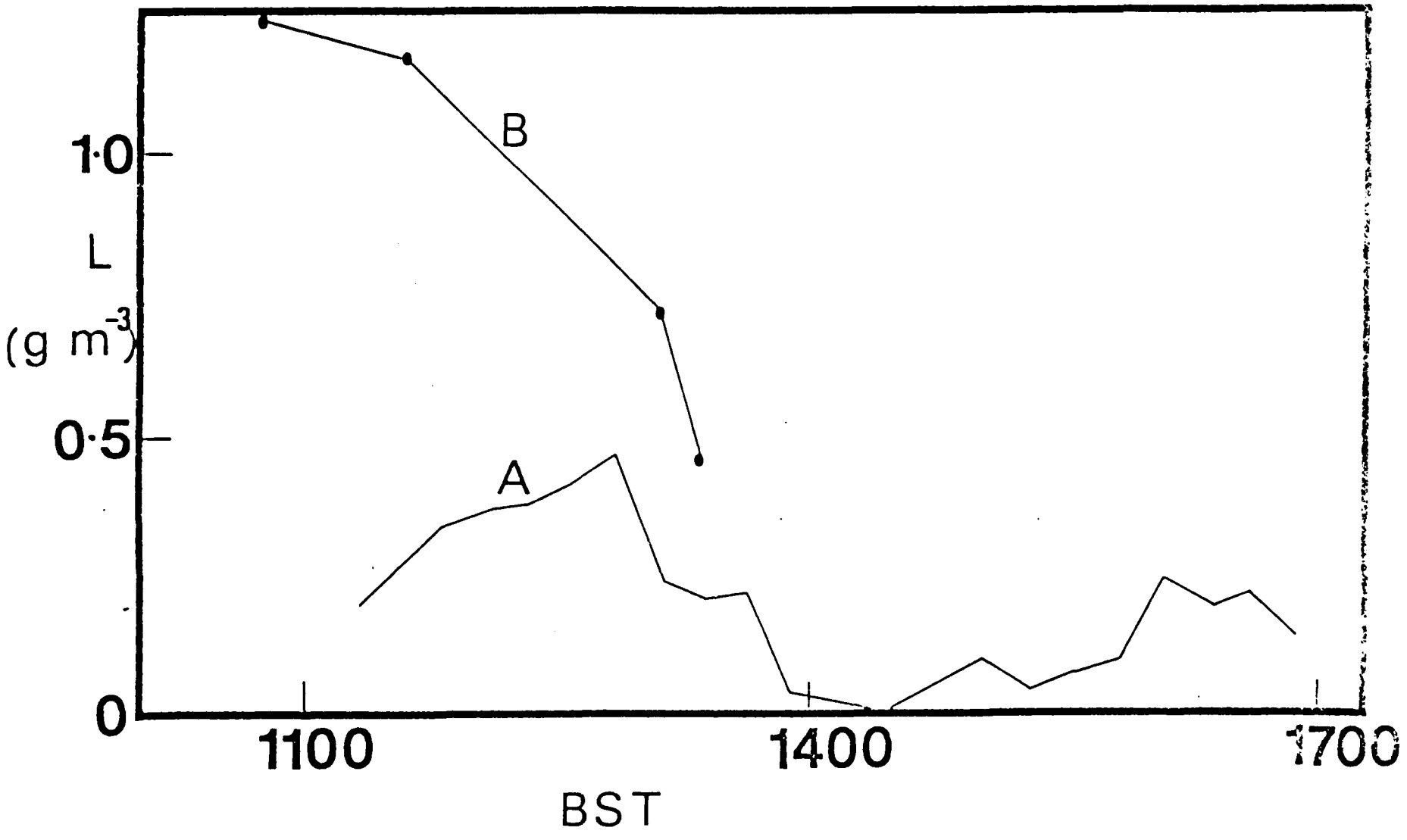

Figure 11

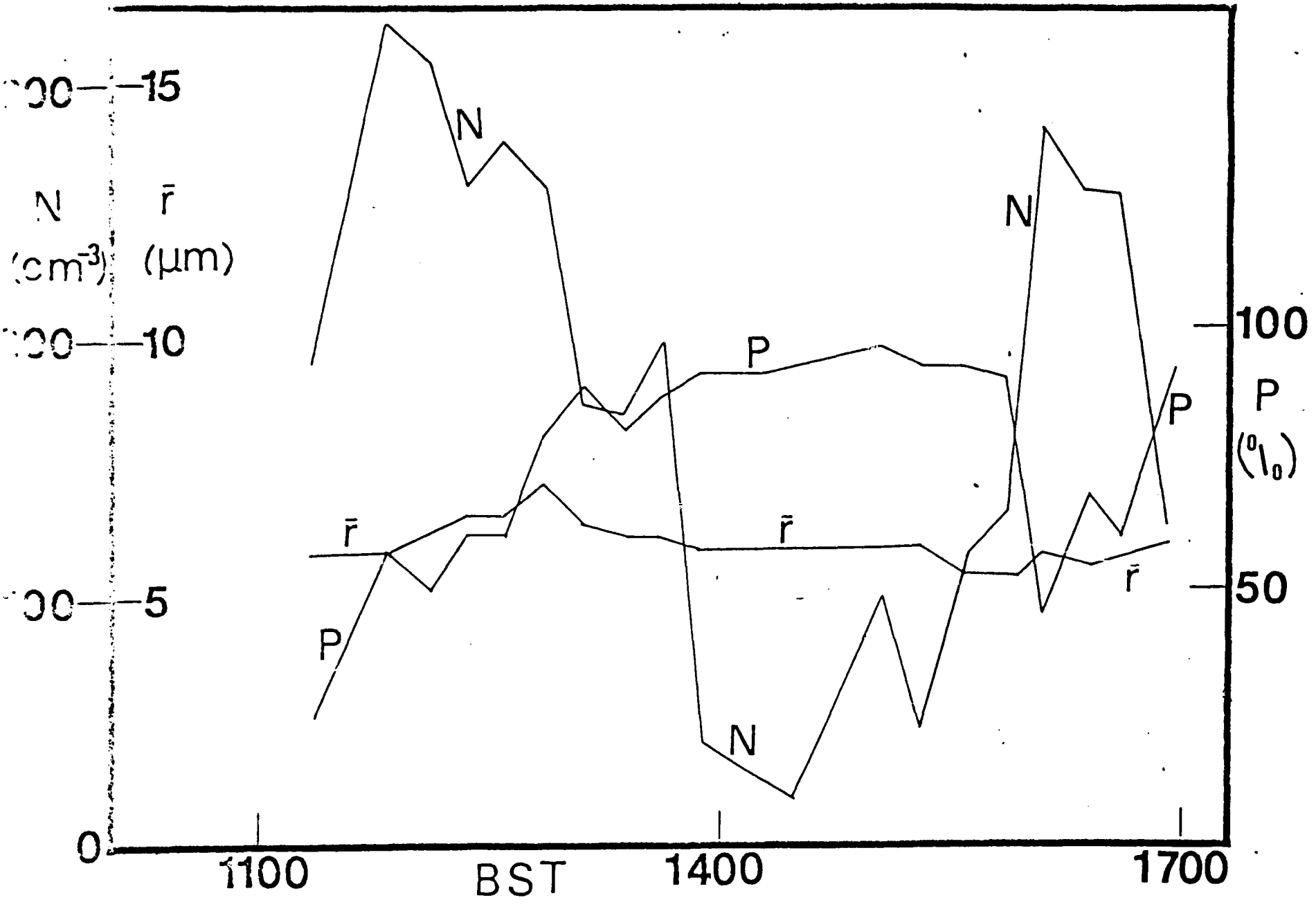
00
15
N
r̄
(cm⁻³)
(μm)
00
10
00
5
0
N
N
P
P
r̄
r̄
r̄
P
N
100
P
(⁰I₀)
50
1100
BST
1400
1700

Figure 12

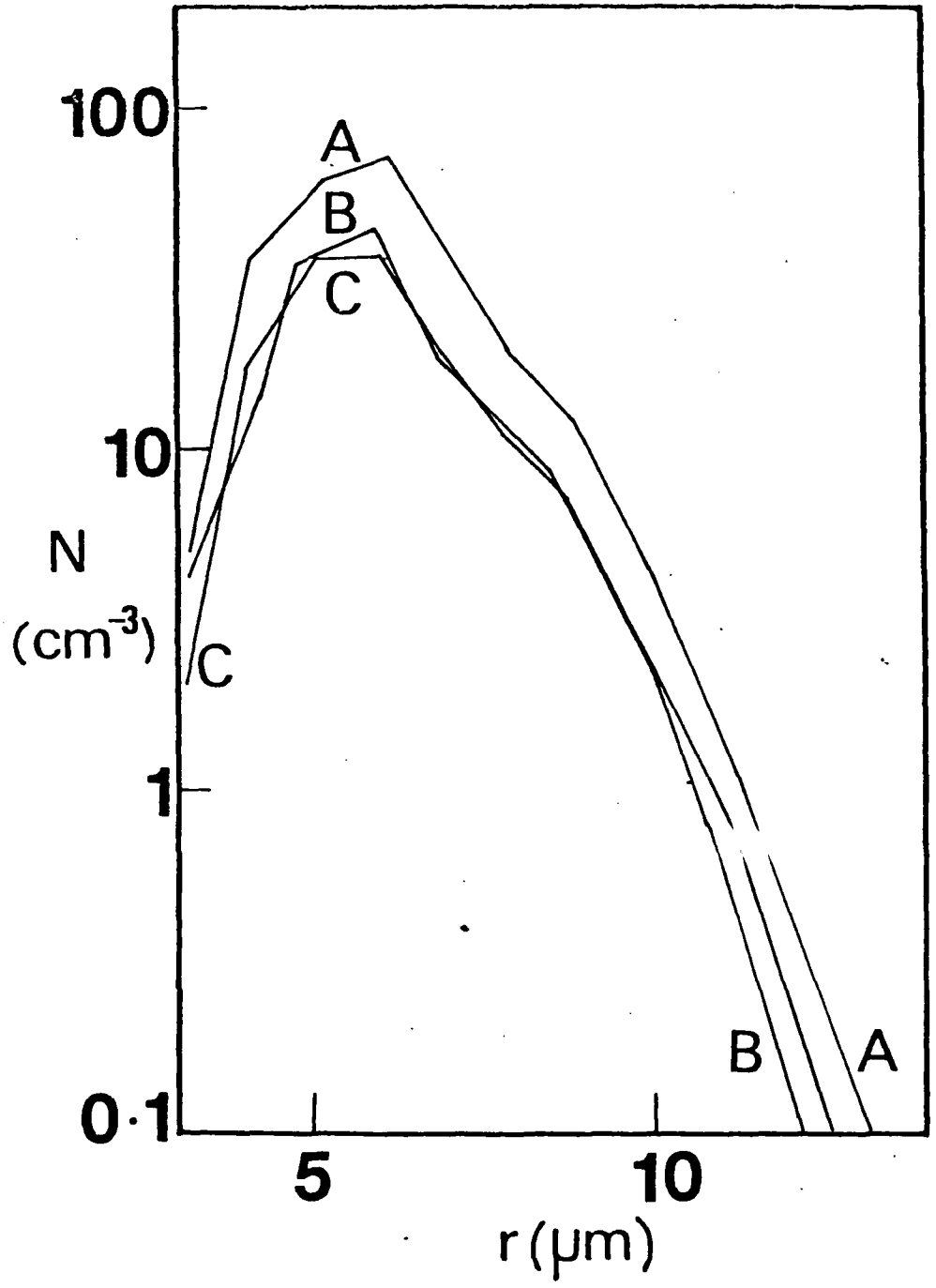

Figure 13

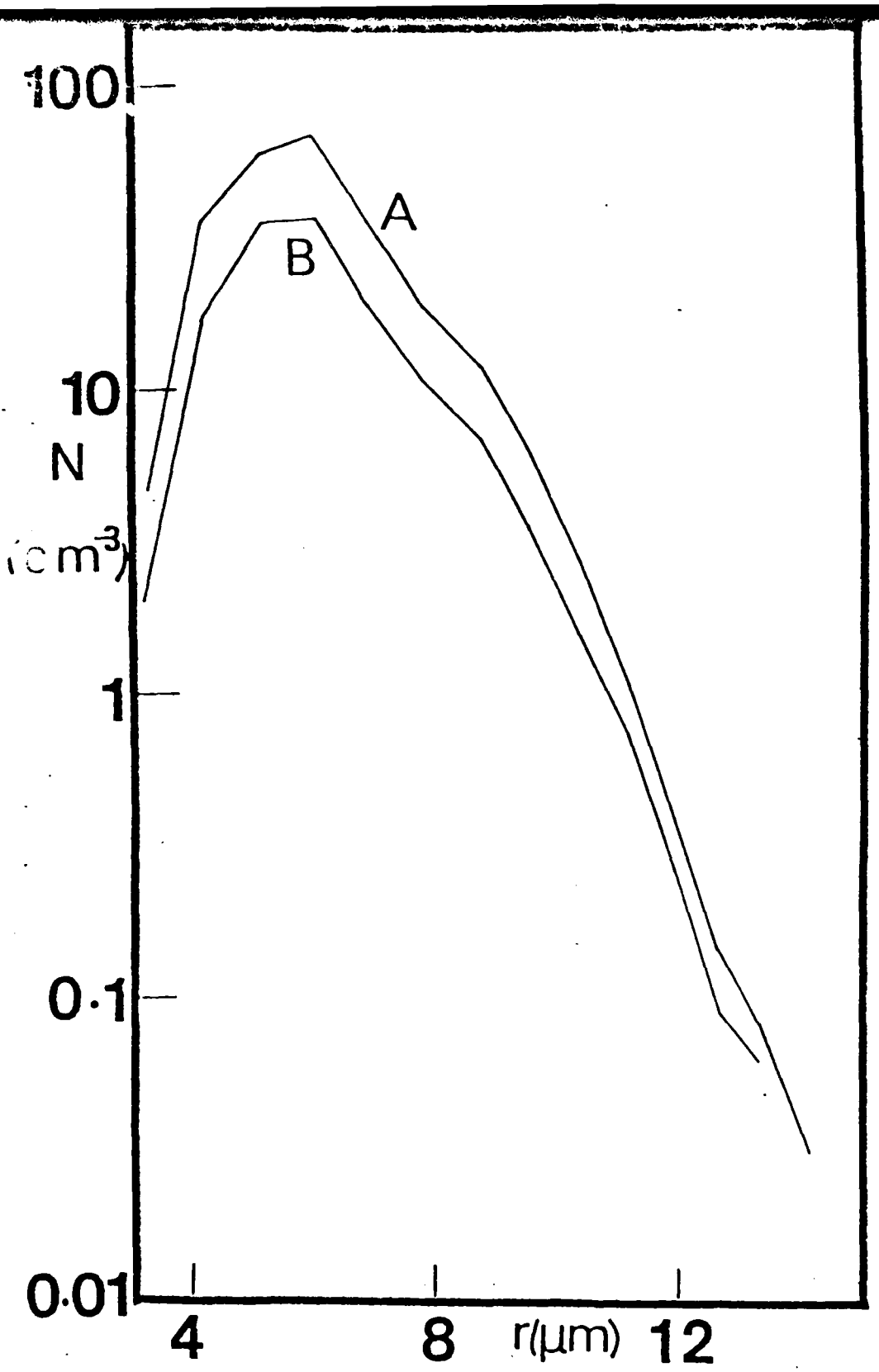

Figure 14

III. INFRA-RED ATTENUATION IN LIMITED VISIBILITY CONDITIONS

Introduction

Simultaneous measurements of the attenuation of infra-red radiation, cloud droplet size spectra and cloud liquid water content have recently been made at the summit of Great Dun Fell. Preliminary analysis of these data suggests that this attenuation at about 11μm may be predicted from measurements of cloud liquid water content by means of the Chylek relationship to a reasonable degree of accuracy. Good temporal correlation of extinction coefficient values derived from transmissometer measurements with those derived from cloud liquid water contents clearly exists and further analysis is being conducted in an endeavour to establish the likely errors in the extinction coefficient measurements arising from factors such as multiple scattering within the transmission path.

Field Measurements

A Barnes Model 14 Infra-red transmissometer system available under a collaborative research agreement with Royal Signals and Radar Establishment at Malvern was operated utilizing a total transmission path length of 41.5 metres. The transmission measurements were made utilizing a spike filter centred at 10.9μm $\pm$ 0.3μm though the instrument is also capable of operating over 3-5μm or 8-13μm radiation bands. It was considered that the nominal angular field of view of 3 milliradians for the radiation receiver with the associated very small detector size rendered insignificant any forward scattering corrections which are neglected for the purposes of data analysis. Simultaneous measurements of cloud droplet spectra were made with a PMS FSSP instrument which is capable of sizing droplets of 3 to 47μm in diameter. In addition, direct measurements of cloud liquid water content were made with an optical scattering instrument developed at UMIST which possesses a sample volume of a few millilitres and a path length of approximately 0.2 metres. For ground-based usage, the FSSP is fitted with an intake horn and an aspirator fan which provides an aspiration velocity of about 26 metres per second through the sampling region and an overall volume sampling rate of 8.14 ml s^{-1}. It became apparent during these field studies that winds in excess of about 15 m s^{-1} exerted a 'ram' effect upon the intake horn of the FSSP resulting in significant increases in the volume flow rate of air through the instrument and consequent overestimation of droplet number concentrations. Limited investigation of this phenomenon suggested that moderate wind speeds, of less than about 10m s^{-1}, did not significantly influence droplet number concentration measurements but that overestimations by as much as a factor of 4 might occur with wind velocities approaching 20m s^{-1}. The

optical scattering instrument proved suitable for ground-based operation in situations where cloud liquid water contents in excess of about 0.05g m^{-3} were encountered. Its bandwidth of about 1KHz and its small sample volume made it extremely responsive to small scale fluctuations in liquid water content.

Preliminary Data Analysis

Data from the Barnes transmissometer was recorded in analogue form on a chart recorder and values of extinction coefficient for a given cloud sample were calculated by taking 20s averages of the chart record in order to correspond with droplet size and number concentration spectra obtained from the FSSP over the same time intervals. These spectra were integrated to provide a series of measurements of cloud liquid water content. Chylek (1978) suggested that extinction coefficient, σ_e, could be related to liquid water content, W, by means of the relationship

$$\sigma_e = \frac{3\pi C}{2\rho\lambda} W$$

where C is a constant for a given experimental situation, ρ is the water density and λ is the wavelength of the radiation. Thus, values of extinction coefficient obtained by utilizing this formula could be compared with values derived from direct transmission measurements, A typical sample of data obtained by this method is plotted in Figure 1 and exhibits a strong temporal correlation between the extinction coefficient curves provided allowance is made for the FSSP sampling errors. Clearly the FSSP correction factor is not sufficiently well defined to be very meaningful here and demonstrates the need for more detailed calibration studies. The close temporal correlation is nevertheless remarkable when the extended sample volume of the transmissometer is compared with that of the FSSP, and serves to support the validity of this experimental approach.

Figure 2 shows a comparison of extinction coefficients from attenuation measurements compared with ones derived from liquid water content measurements made with the optical scattering device again using the Chylek formula. Unfortunately, the

period analysed does not exhibit a very wide range of values of extinction coefficient but nevertheless a reasonable degree of correlation between the two sets of measurements may be noted.

Multiple scattering errors arise when radiation scattered out of the transmitted beam is re-scattered into the beam by interaction with another particle. This multiple scattering is increased as the number of scatterers is increased whether by a greater concentration of particles per unit volume or by an extended path length and its effect must be to enhance the transmission of radiation through the medium compared with that predicted from the liquid water content measurements. More detailed study of the data from the field measurements does indeed support this hypothesis and a simple scheme whereby a corrected extinction coefficient, σ_e', is derived from the measured coefficient utilizing a formula of the type

$$\sigma_e' = \sigma_e(1 + \alpha N^2)$$

where N is the droplet number concentration and α is a constant for a given experimental configuration, does appear to yield much closer agreement between the calculated and measured values. A sample of data treated in this manner is reproduced in Figure 3. This approach is rather rudimentary at present and a much more detailed treatment is required.

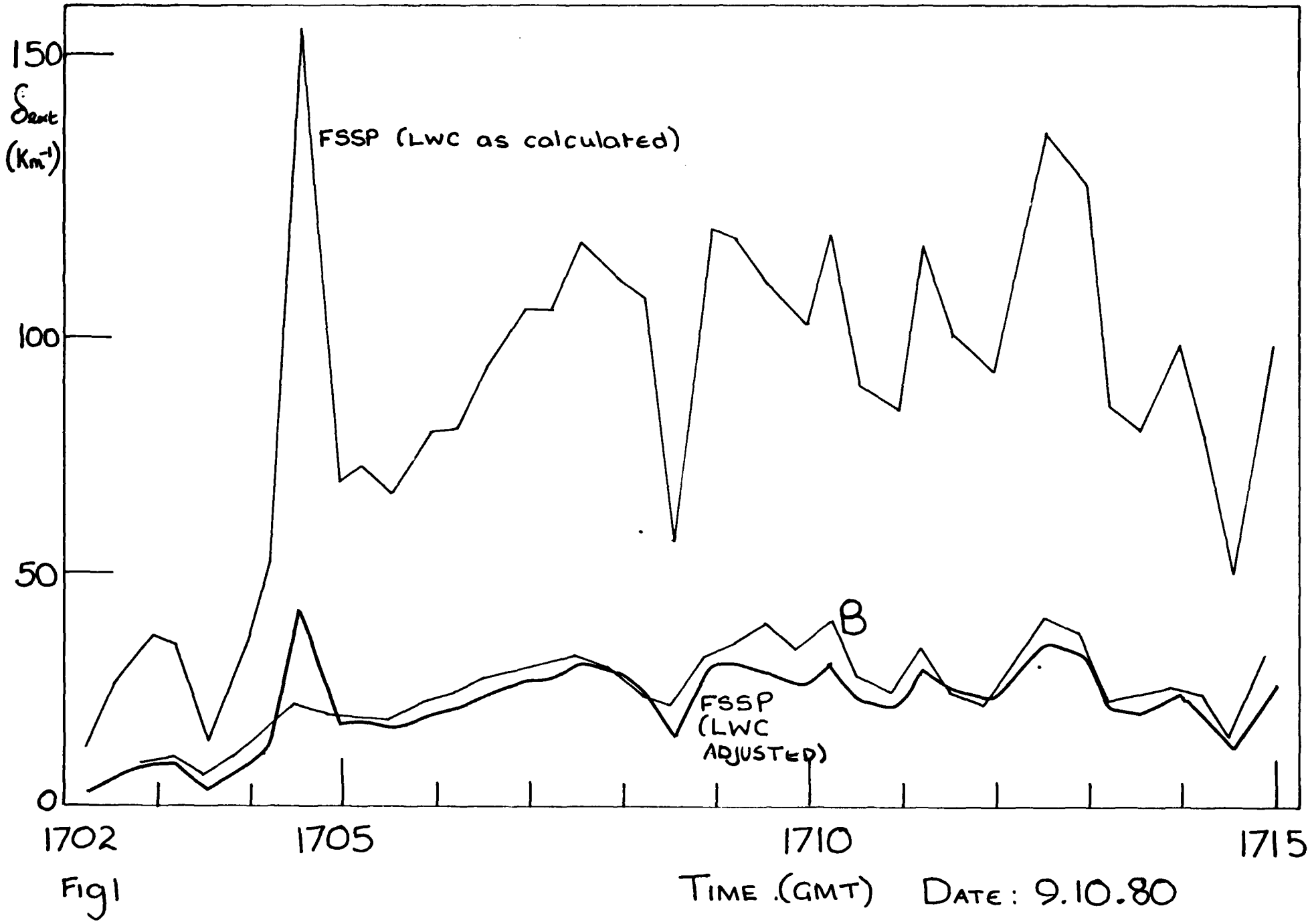
150
σ_{ext}
(Km^{-1})
100
50
0
FSSP (LWC as calculated)
B
FSSP
(LWC
ADJUSTED)
1702
1705
1710
1715
TIME (GMT)
DATE: 9.10.80

Fig1

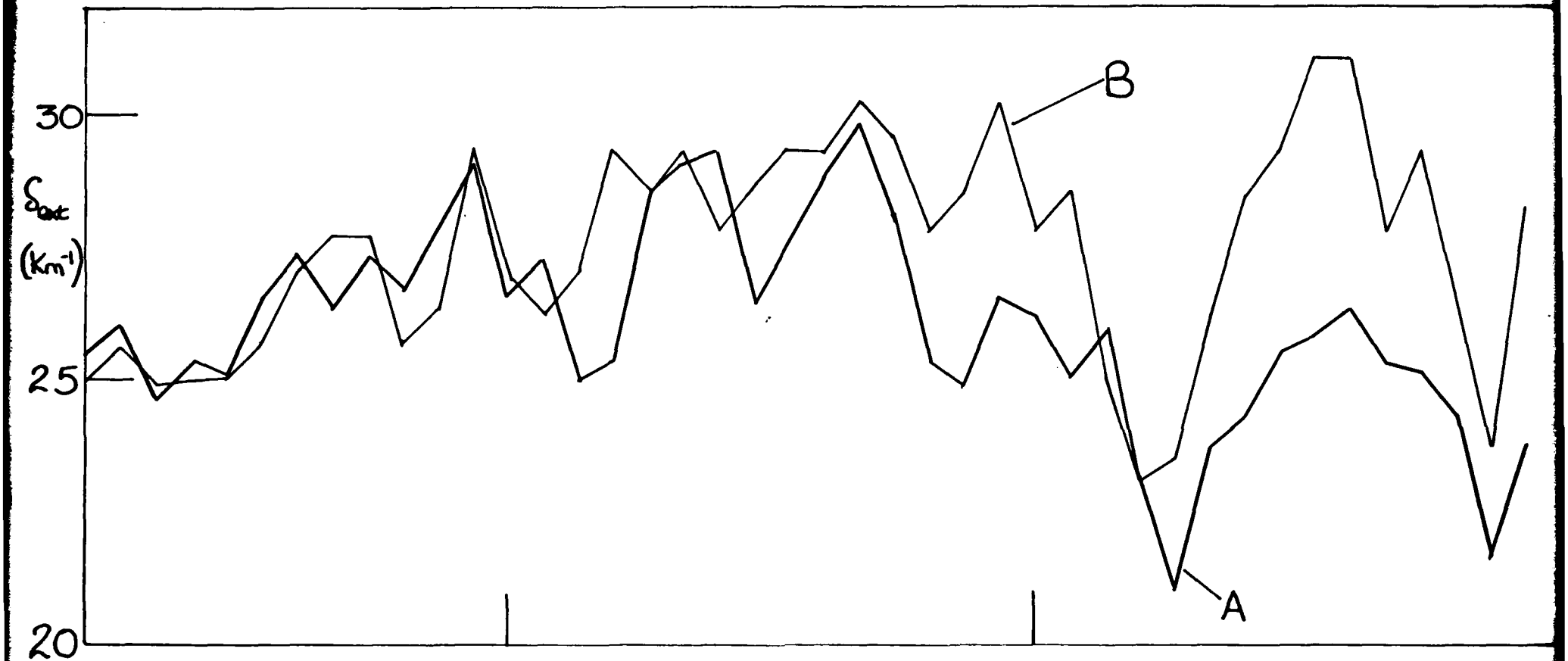
30
25
20
σ_{ext}
(km^{-1})
B
A
1916
1920
Time (GDF)
1925
Date: 9.10.80
A: He-Ne LWC Device
B: Barnes Transmissometer
Path Length 41.5m

Fig 2

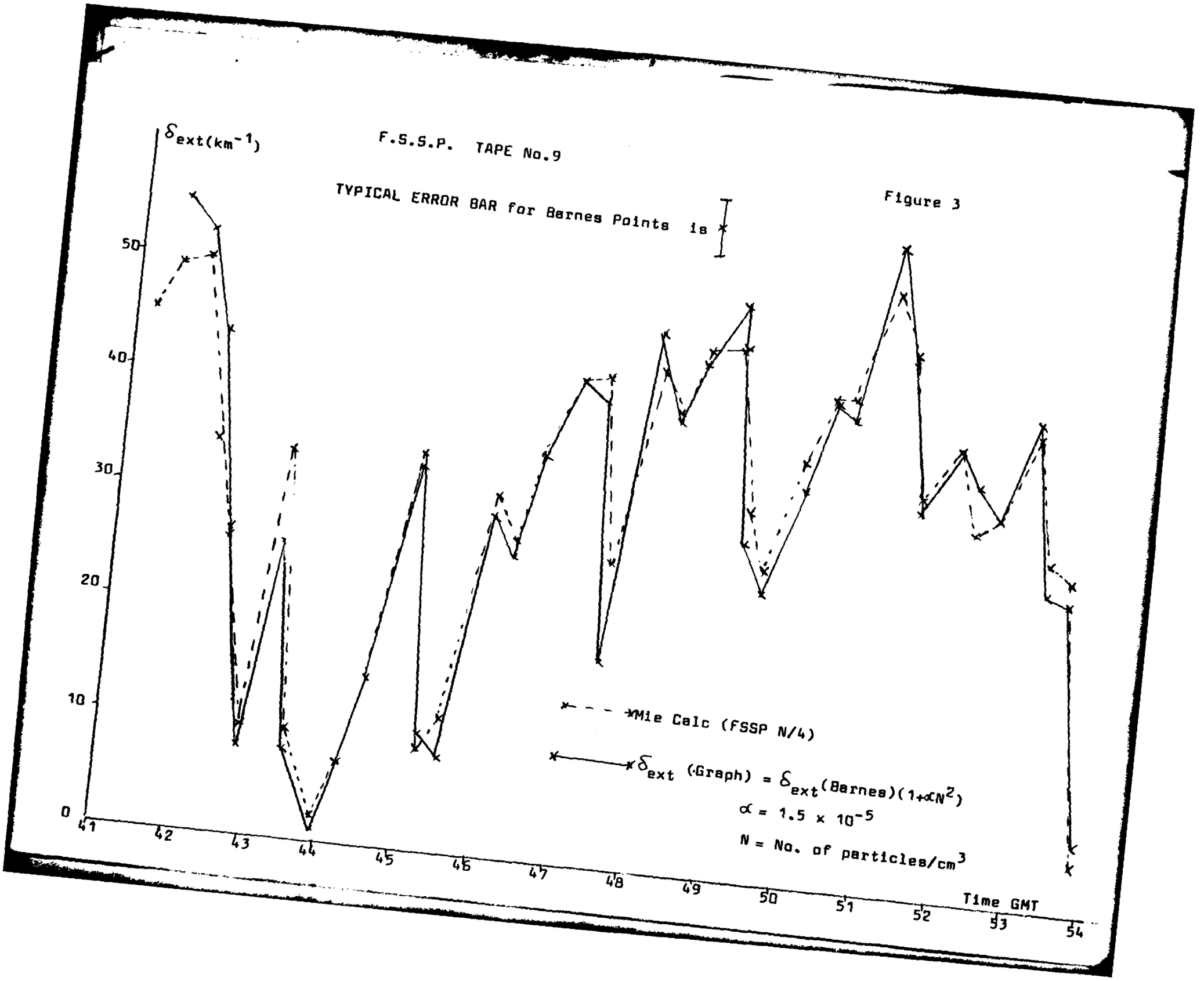
$\delta_{ext(km^{-1})}$
F.S.S.P. TAPE No.9
TYPICAL ERROR BAR for Barnes Points is
Figure 3
50
40
30
20
10
0
41
42
43
44
45
46
47
48
49
50
51
52
53
54
Time GMT
Mie Calc (FSSP N/4)
δ_{ext} (Graph) = δ_{ext}(Barnes)$(1+\alpha N^2)$
$\alpha = 1.5 \times 10^{-5}$
N = No. of particles/cm^3


F
6